Supporting Information

Single and Dual Metal Atom Catalysts for Enhanced Singlet Oxygen Generation and Oxygen Reduction Reaction

Mohsen Tamtaji[1], Songhhua Cai[2], Wenting Wu[3], Tongchao Liu[4], Zhimin Li[2], Hsun-Yun Chang[5], Patrick Ryan Galligan[1], Shin-ichi Iida[5], Xiangrong Li[1], Faisal Rehman[1,6], Khalil Amine[4], William A. Goddard III[6*], and Zhengtang Luo[1*]*

[1]Department of Chemical and Biological Engineering, Guangdong-Hong Kong-Macao Joint Laboratory for Intelligent Micro-Nano Optoelectronic Technology, William Mong Institute of Nano Science and Technology, and Hong Kong Branch of Chinese National Engineering Research Center for Tissue Restoration and Reconstruction, The Hong Kong University of Science and Technology, Clear Water Bay, Kowloon, Hong Kong, 999077, P.R. China

[2]Department of Applied Physics, The Hong Kong Polytechnic University, Hunghom, Kowloon 999077, Hong Kong

[3]State Key Laboratory of Heavy Oil Processing, College of Chemistry and Chemical Engineering, Institute of New Energy, China University of Petroleum (East China), Qingdao 266580 (P. R. China)

[4]Chemical Sciences and Engineering Division Argonne National Laboratory 9700 Cass Ave, Lemont, IL 60439, USA

[5]ULVAC-PHI, Inc., Analytical Laboratory, 2500 Hagisono, Chigasaki, Kanagawa 253-8522, Japan

[6]Materials and Process Simulation Center (MSC), MC 139-74, California Institute of Technology, Pasadena CA, 91125, USA

Corresponding authors email: keztluo@ust.hk, amine@anl.gov, and wag@caltech.edu

Number of pages: 33

Number of Figures: 28

Number of Tables: 3

1 **Table of contents**

2

3

S1. Characterization

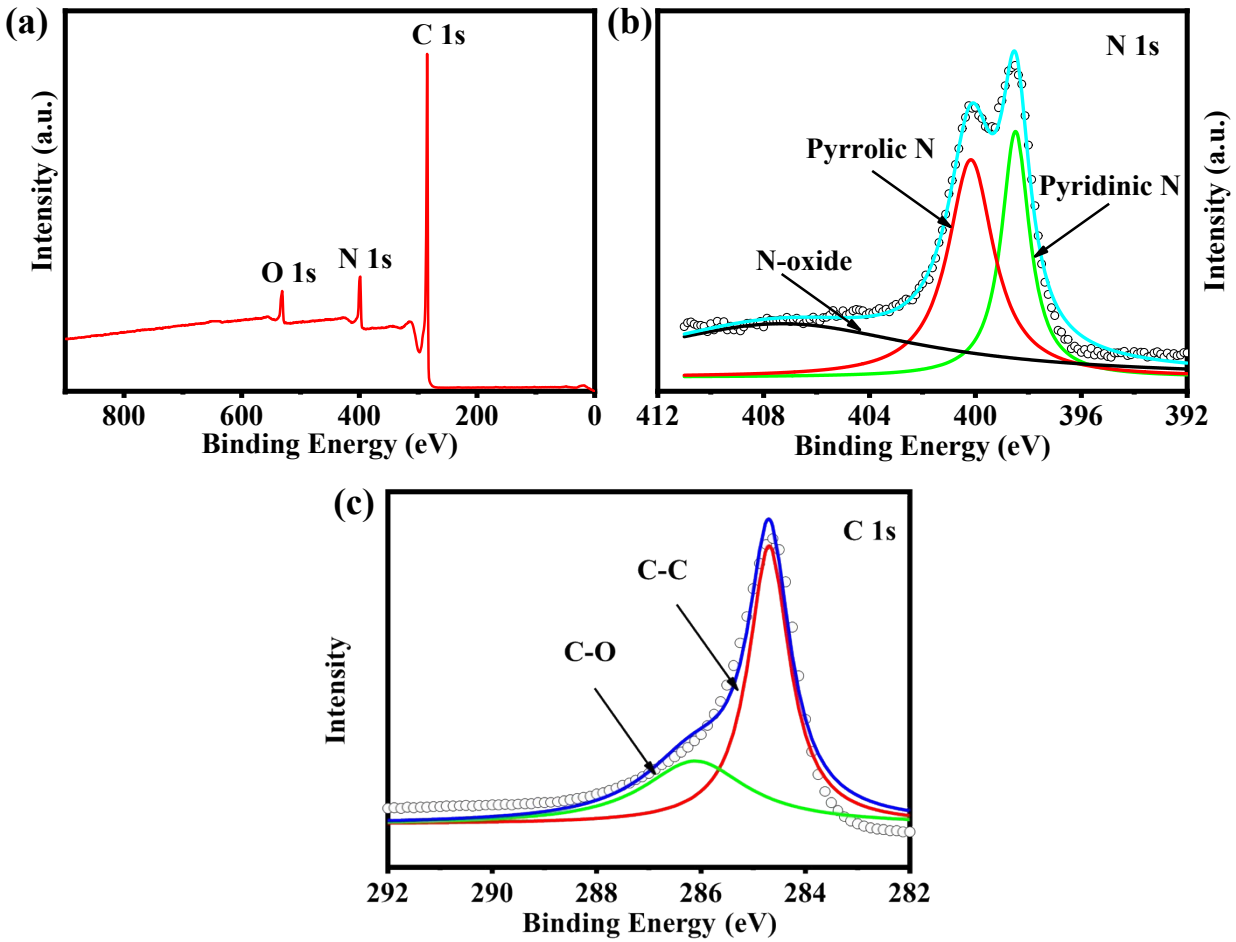

Figure S1. XPS results for N-doped sample. (a) Wide range XPS spectra of N-doped sample. (b) The N 1s XPS spectra of the N-doped sample with three visible N species belong to pyridinic-N (398.5 eV), pyrrolic-N (400.2 eV), and oxidized-N (407.3 eV). (c) The C 1s XPS spectra of the N-doped sample with two visible C species belong to C-C (284.7 eV) and C-O (286.1 eV).

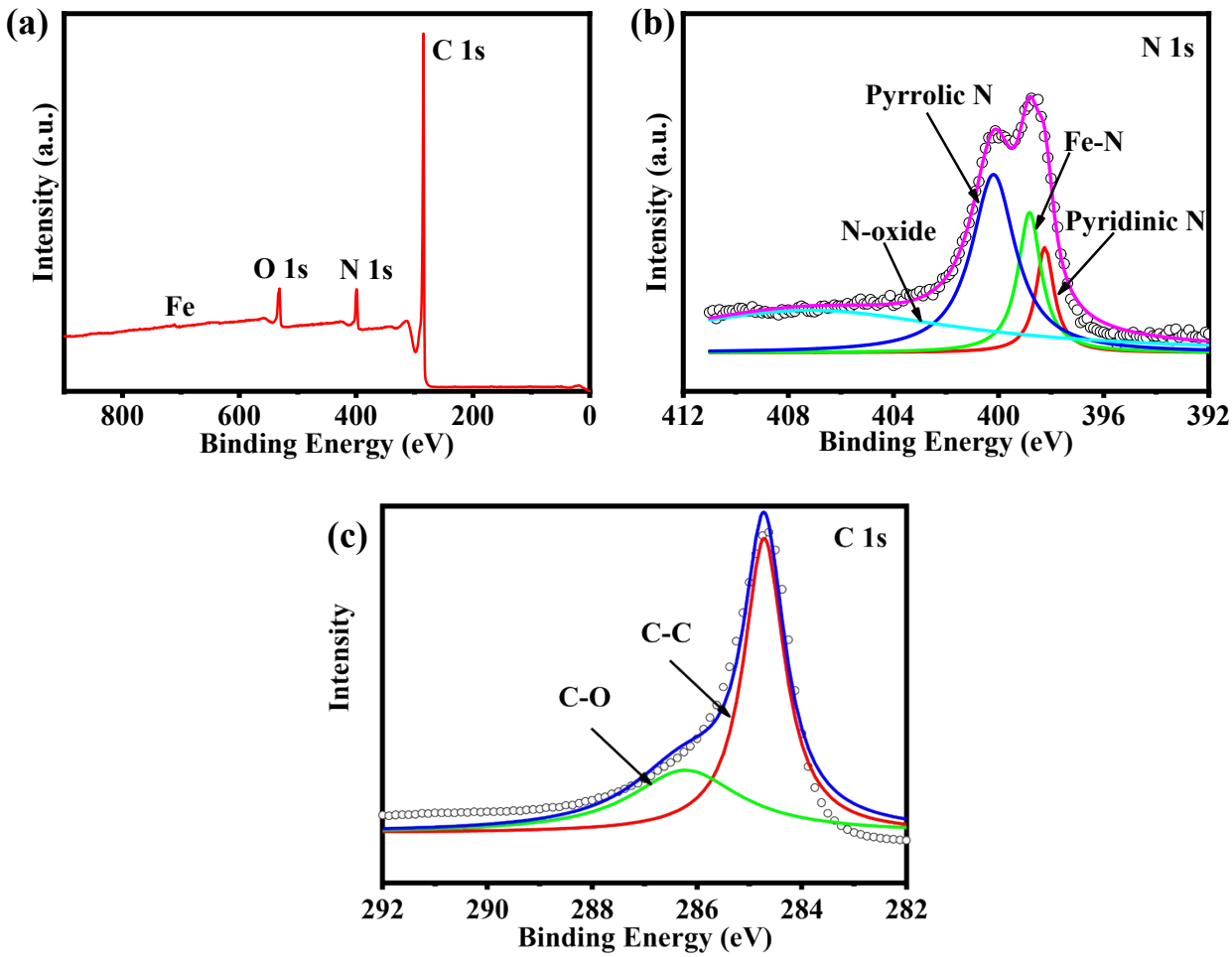

Figure S2. XPS results. (a) Wide range XPS spectra of FeN4-SAC sample. (b) The N 1s XPS spectra of the FeN4-SAC sample with four visible N species belong to pyridinic-N (398.2 eV), Fe-N (398.8 eV), pyrrolic-N (400.2 eV), and oxidized-N (407.1 eV). (c) The C 1s XPS spectra of the FeN4-SAC sample with two visible C species belong to C-C (284.7 eV) and C-O (286.2 eV).

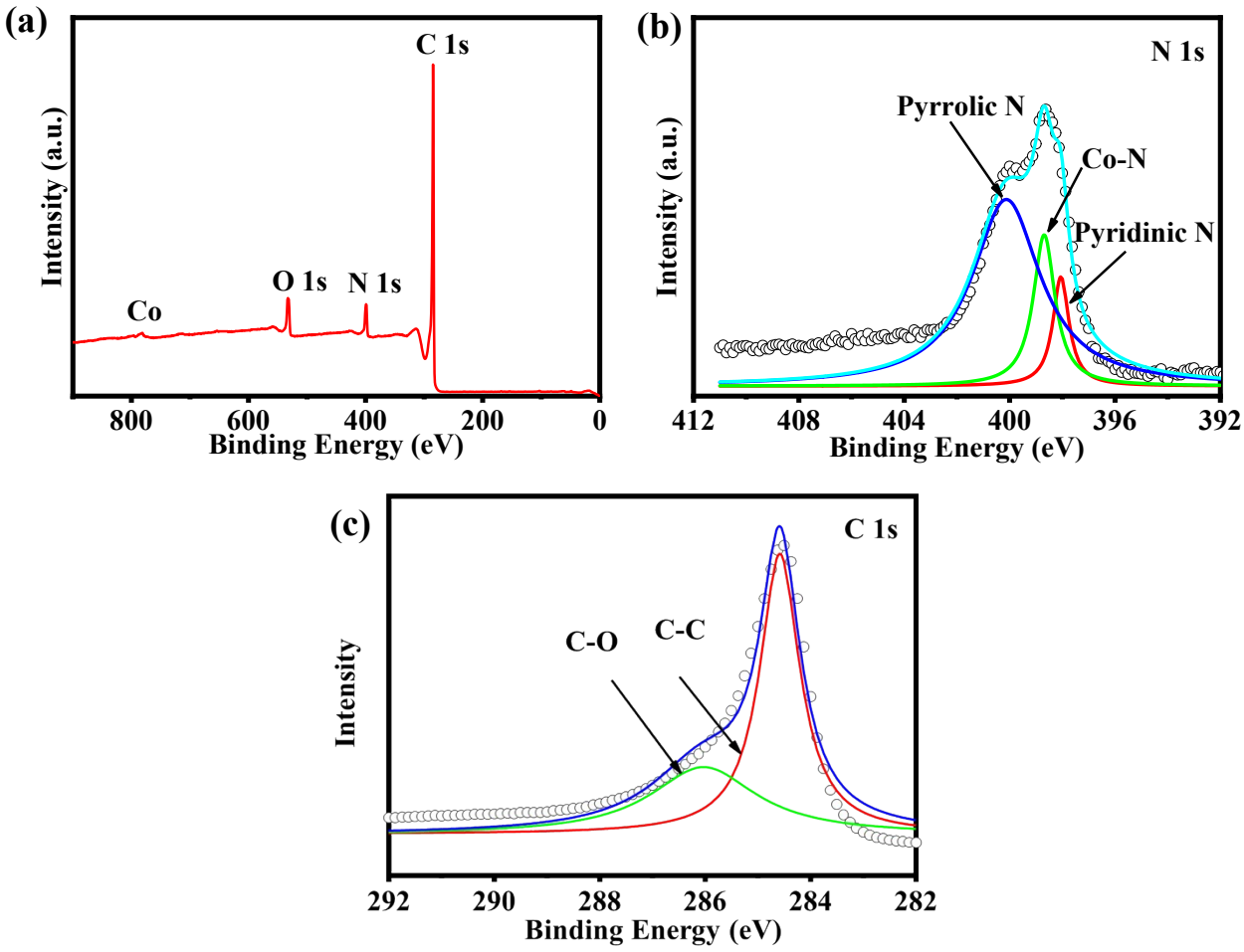

Figure S3. XPS results. (a) Wide range XPS spectra of CoN4-SAC sample. (b) The N 1s XPS spectra of the CoN4-SAC sample with three visible N species belong to pyridinic-N (398.0 eV), Co-N (398.7 eV), and pyrrolic-N (400.1 eV). (c) The C 1s XPS spectra of the CoN4-SAC sample with two visible C species belong to C-C (284.6 eV) and C-O (286.0 eV).

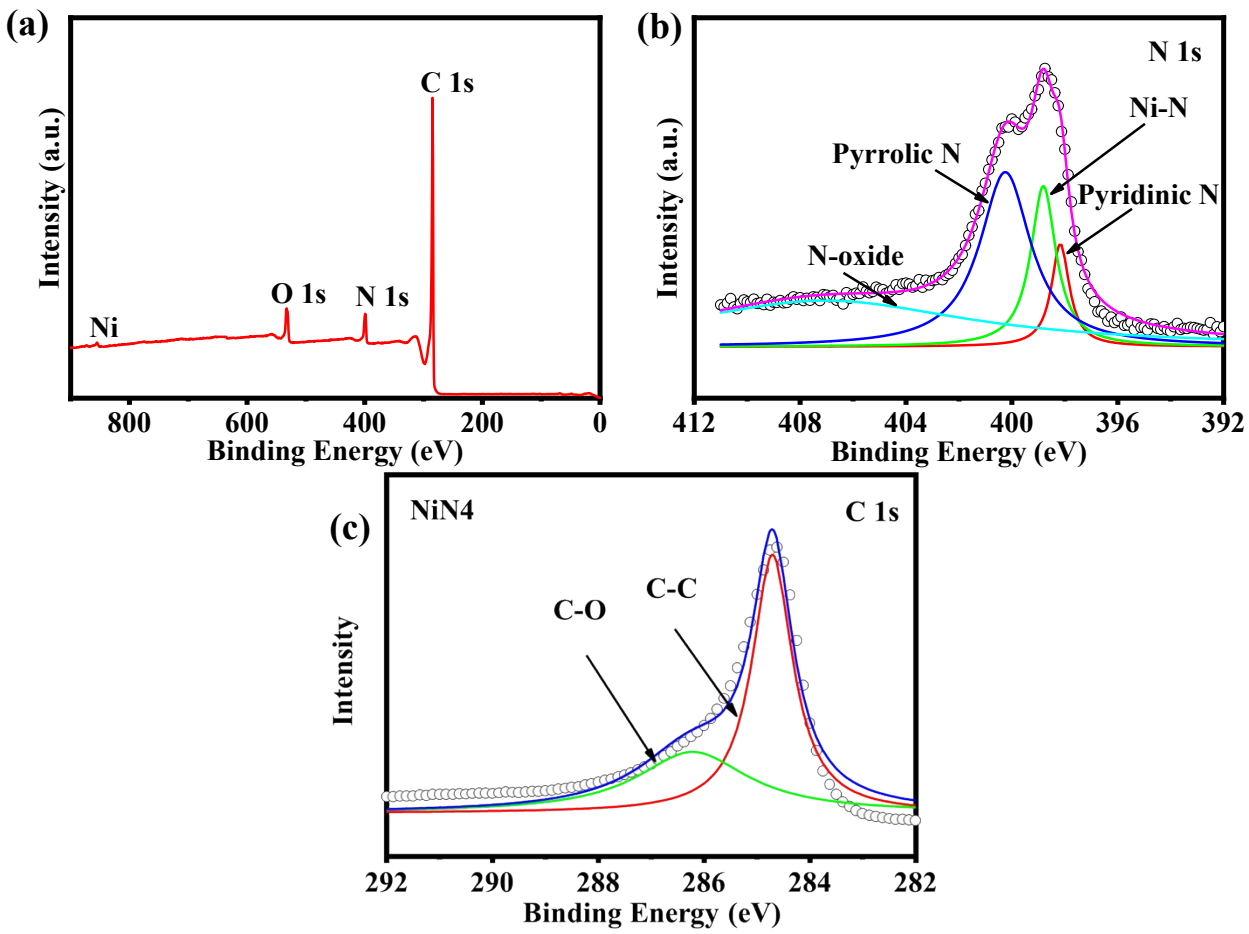

Figure S4. XPS results. (a) Wide range XPS spectra of NiN4-SAC sample. (b) The N 1s XPS spectra of the NiN4-SAC sample with four visible N species belong to pyridinic-N (398.2 eV), Ni-N (398.8 eV), pyrrolic-N (400.2 eV), and oxidized-N (407.0 eV). (c) The C 1s XPS spectra of the NiN4-SAC sample with two visible C species belong to C-C (284.7 eV) and C-O (286.2 eV).

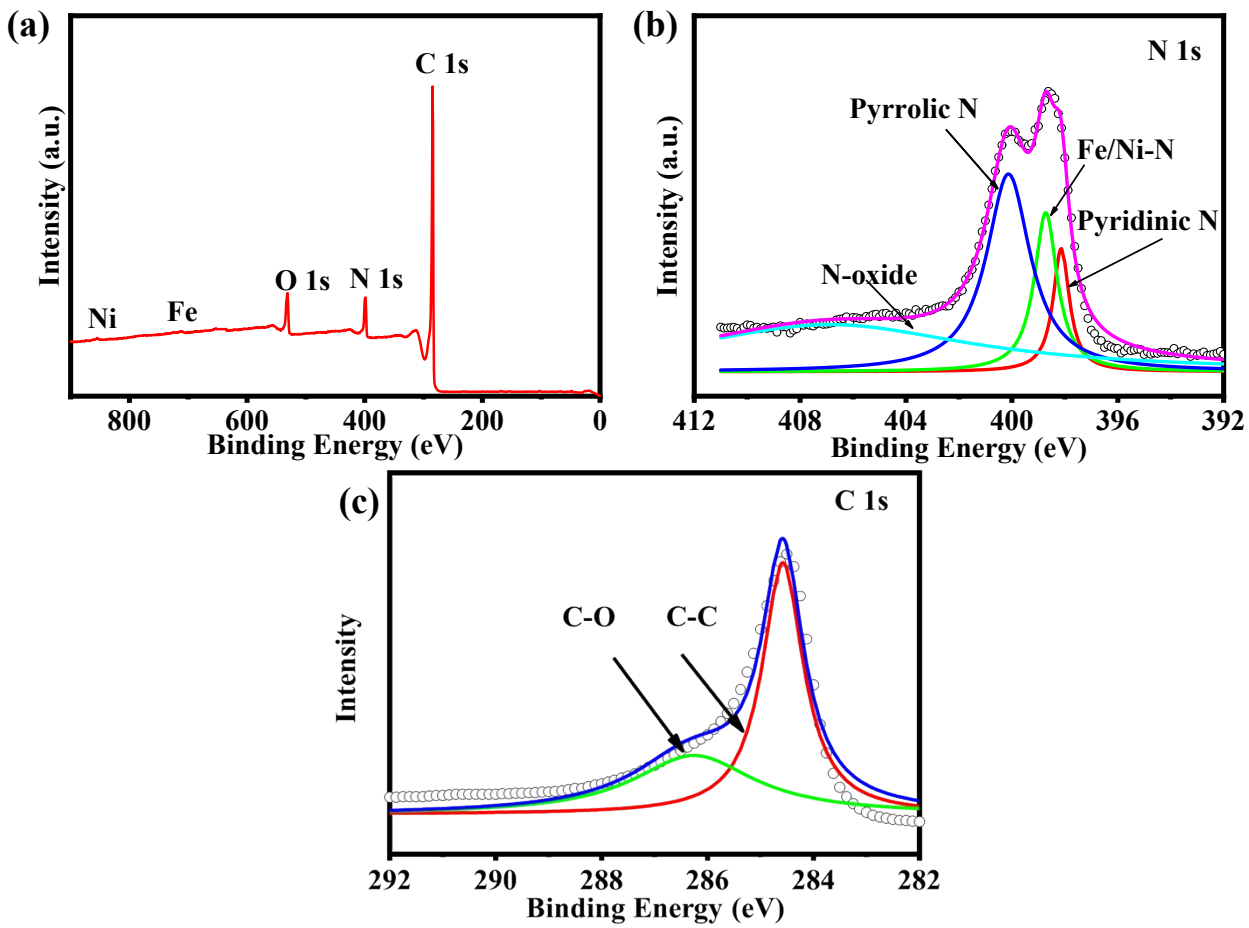

Figure S5. XPS results. (a) Wide range XPS spectra of FeNiN8-DAC sample. (b) The N 1s XPS spectra of the FeNiN8-DAC sample with four visible N species belong to pyridinic-N (398.1 eV), Fe/Ni-N (398.7 eV), pyrrolic-N (400.1 eV), and oxidized-N (406.9 eV). (c) The C 1s XPS spectra of the FeNiN8-DAC sample with two visible C species belong to C-C (284.5 eV) and C-O (286.2 eV).

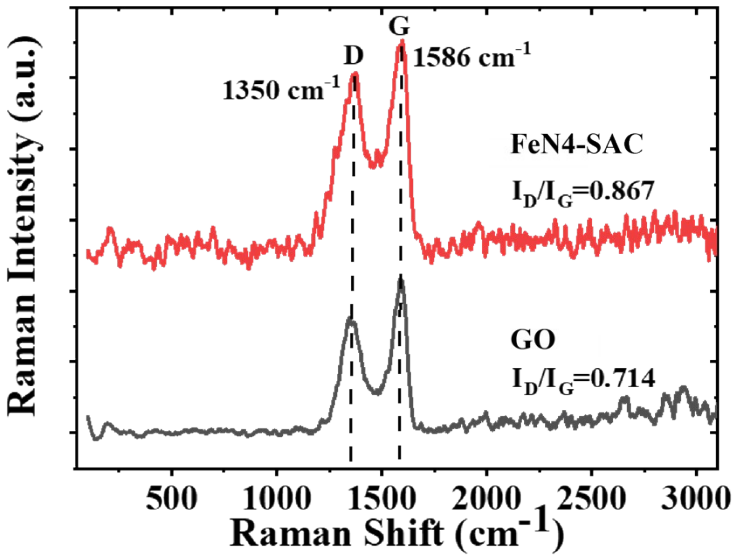

Figure S6. Raman spectroscopy of graphene oxide (GO) and FeN4-SAC. The D peak intensity of the FeN4-SAC sample is increased, indicating the fatty defects nature of the FeN4-SAC sample.

The defect density (n_D) can be calculated using the following equation:[1]

$$n_D(cm^{-2}) = \frac{10^{14}}{\pi^2\left[C_A\left(r_A^2 - r_S^2\right) + C_S r_S^2\right]} \frac{I_D}{I_G}$$

Where for the D peak, the reported values are approximately given as $C_A = 4.2$, $C_S = 0$, $r_A = 3$ nm, and $r_S = 1$ nm,[1] so:

$$n_D = 2.16 \times 10^{11}\, cm^{-2} \qquad for\ GO$$

$$n_D = 2.62 \times 10^{11}\, cm^{-2} \qquad for\ FeN4 - SAC$$

And:

$$n_D = 2.16 \times 10^{-3}\, nm^{-2} \qquad for\ GO$$

$$n_D = 2.62 \times 10^{-3}\, nm^{-2} \qquad for\ FeN4 - SAC$$

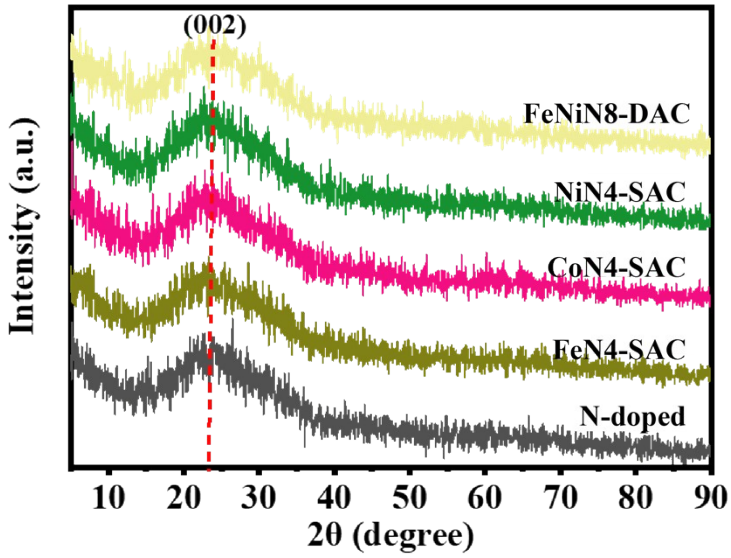

Figure S7. XRD pattern of synthesized N-doped, FeN4-SAC, CoN4-SAC, NiN4-SAC, and FeNiN8-DAC. A peak at 24.1° belongs to the graphitic carbon peak (002). In all the SACs samples, the broad graphitic peak is observed, ensuring the samples' polycrystalline crystal structure. No peak corresponds to metal species in all samples due to a small amount of metal atoms. Based on our XPS measurements, the loading of metal species in each sample is less than 0.4 wt.%.

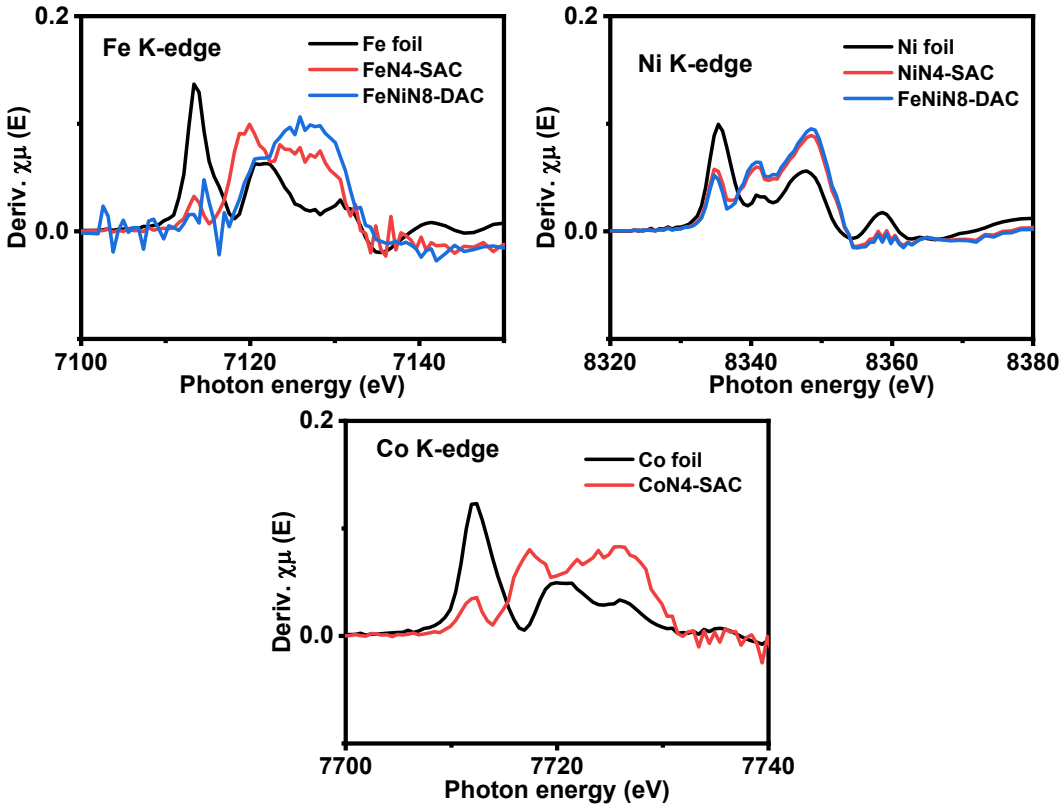

Figure S8. First derivative curves of K-edge XANES spectra with their reference bulk samples.

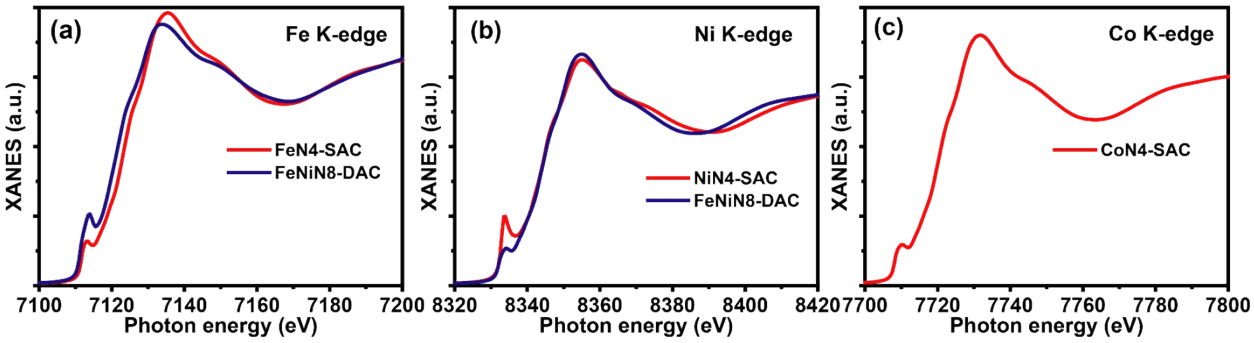

Figure S9. (a) Fe K-edge, (b) Ni K-edge, and (c) Co K-edge XANES spectra of FeN4-SAC, NiN4-SAC, FeNiN8-DAC, and CoN4-SAC, obtained theoretically using accurate finite difference (FD) approach implemented in FDMNES software.

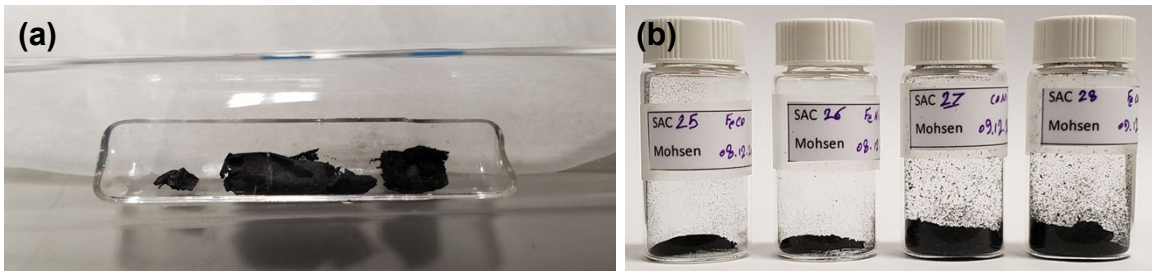

Figure S10. (a) SAC sample after the calcination process. (b) Prepared SAC samples.

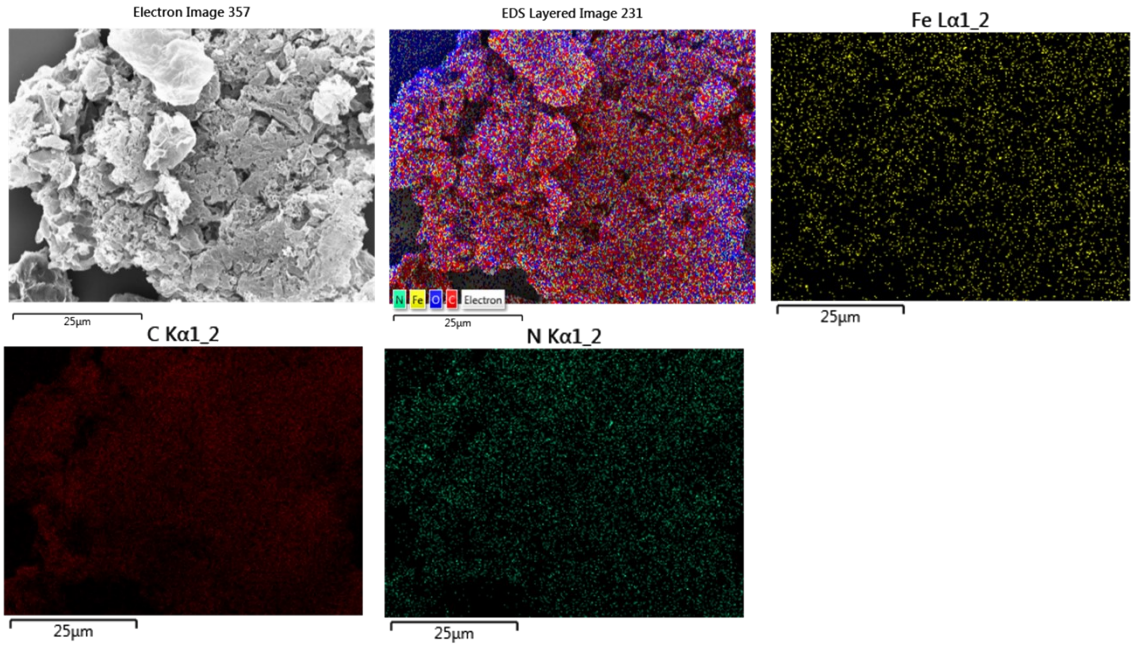

Figure S11. SEM imaging and EDX elemental mapping of FeN4-SAC sample for Fe, C, and N elements.

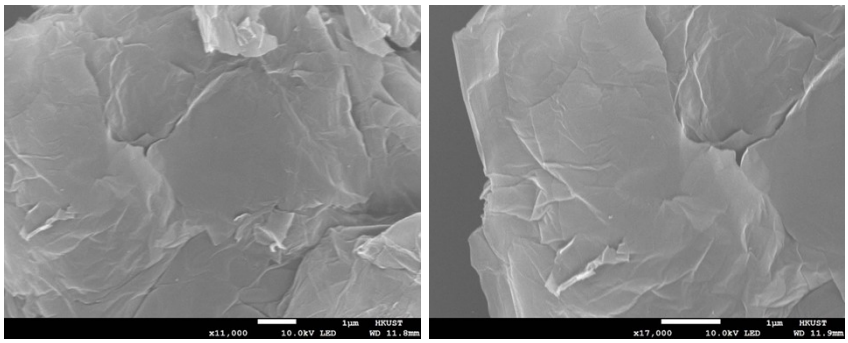

Figure S12. SEM imaging of CoN4-SAC sample.

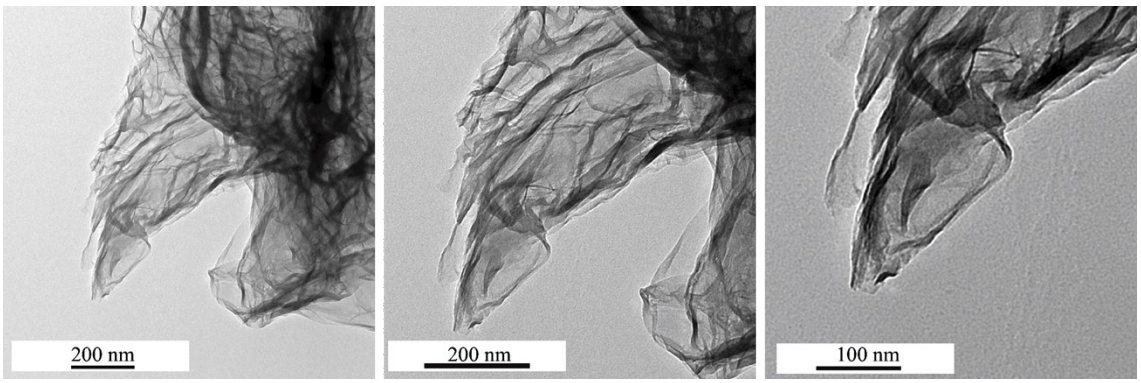

Figure S13. TEM images of FeN4-SAC sample.

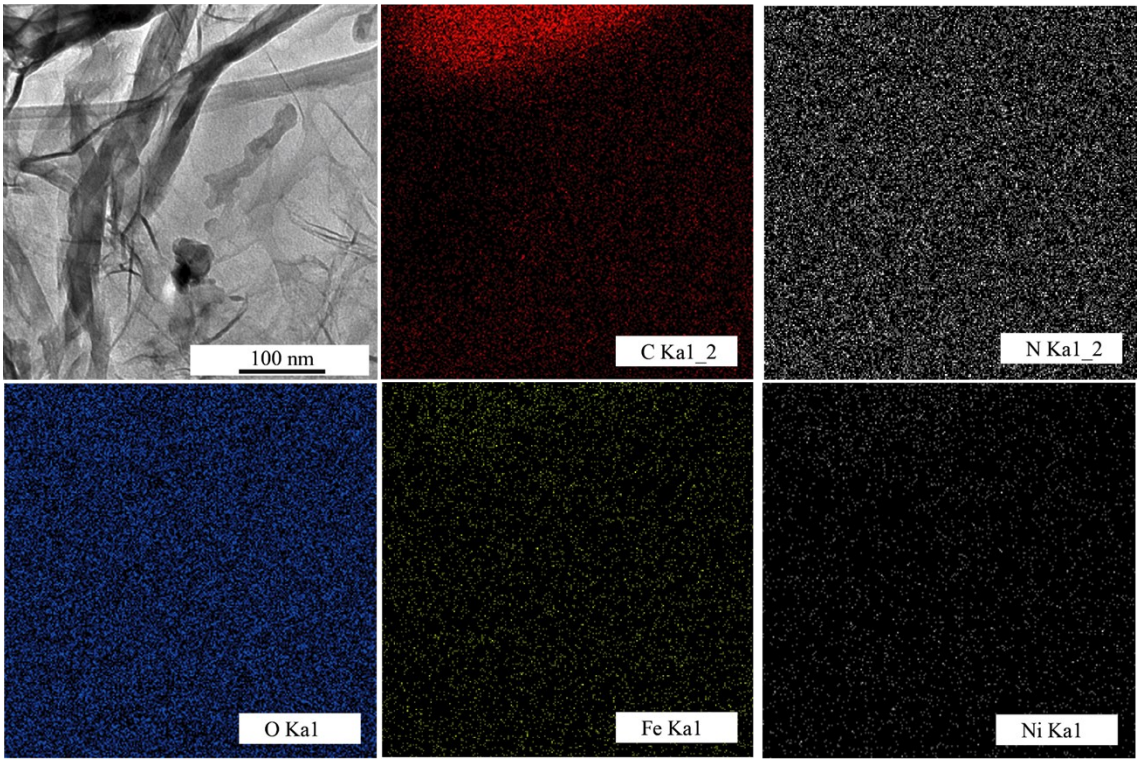

Figure S14. TEM imaging and EDX elemental mapping of FeNiN8-DAC sample for C, N, O, Fe, and Ni elements.

S2. Photocatalytic activity

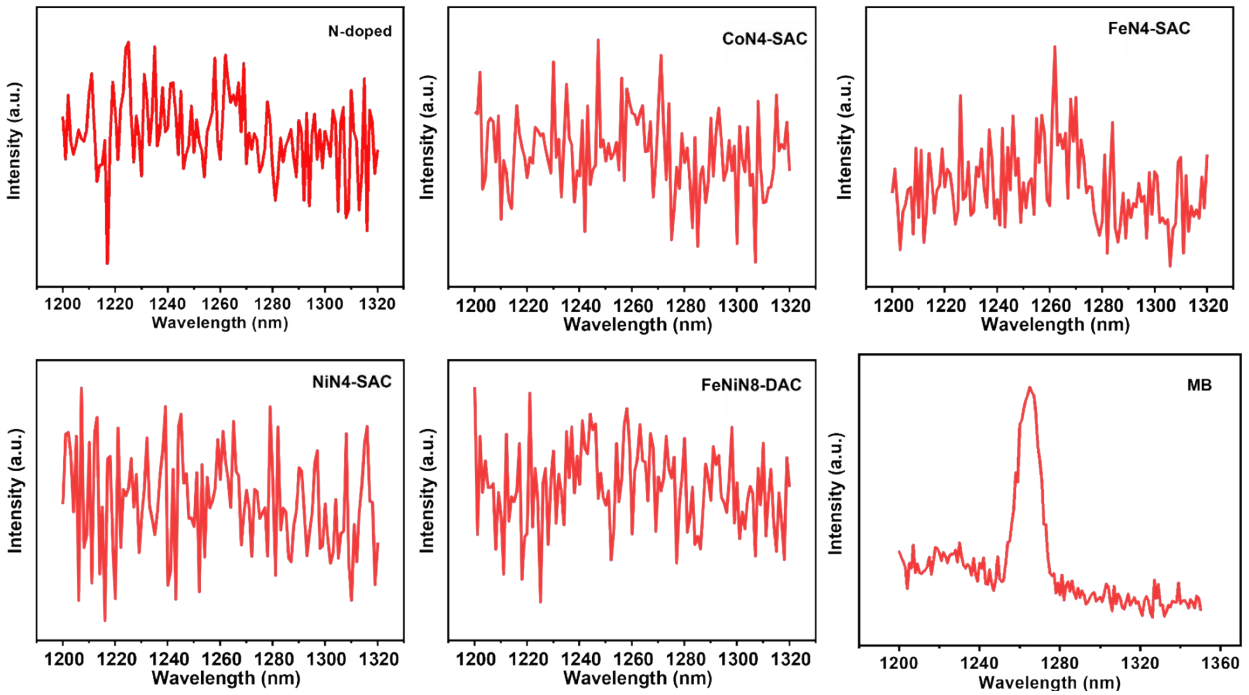

Figure S15. $^1O_2$ emission of N-doped, FeN4-SAC, CoN4-SAC, NiN4-SAC, FeNiN8-DAC, and methylene blue (MB) under excitation with a 532 nm laser. The emission of samples cannot be detected because of the black color of the samples. The characteristic $^1O_2$ emission from methylene blue appeared at 1265 nm, confirming $^1O_2$ generation. The $^1O_2$ emission signal of SACs was detected on a fluorescence spectrometer (FLS980) with a 450 W Xe lamp and a near-infrared (NIR) detector.

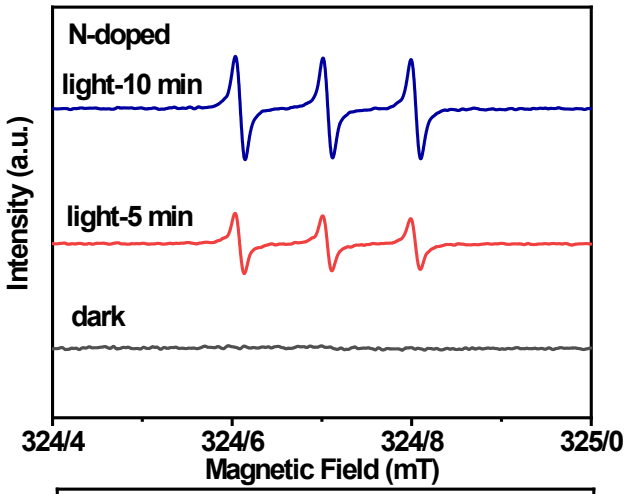
N-doped
light-10 min
light-5 min
dark
Intensity (a.u.)
324/4
324/6
324/8
325/0
Magnetic Field (mT)

FeN4-SAC

1

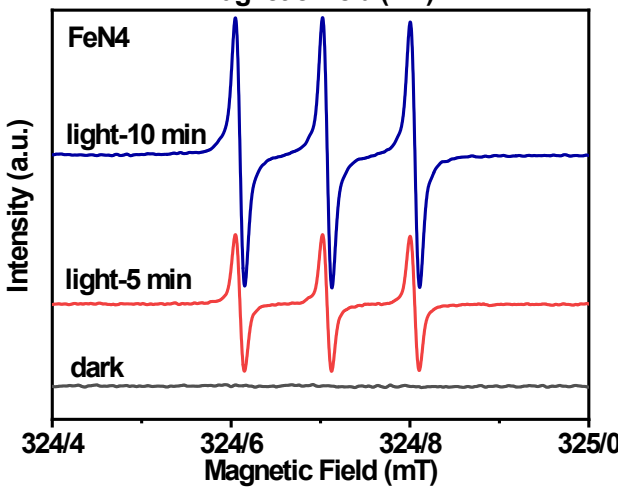
FeN4
light-10 min
light-5 min
dark
Intensity (a.u.)
324/4
324/6
324/8
325/0
Magnetic Field (mT)

2

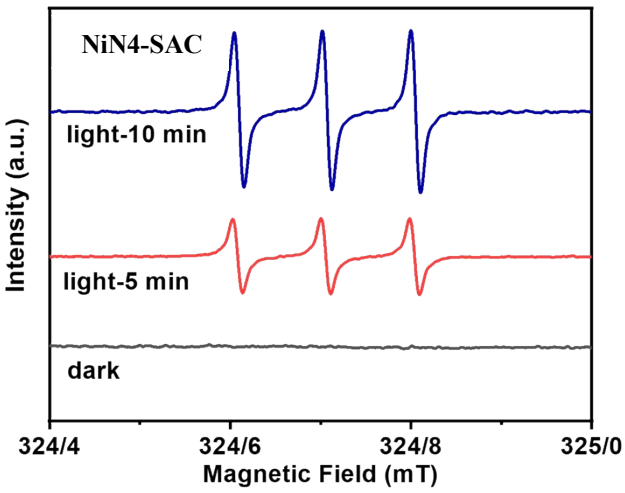
NiN4-SAC
light-10 min
light-5 min
dark
Intensity (a.u.)
324/4
324/6
324/8
325/0
Magnetic Field (mT)

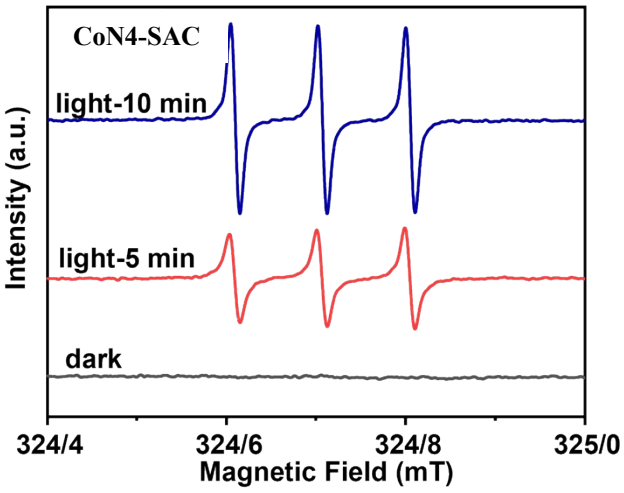
CoN4-SAC
light-10 min
light-5 min
dark
Intensity (a.u.)
324/4
324/6
324/8
325/0
Magnetic Field (mT)

3

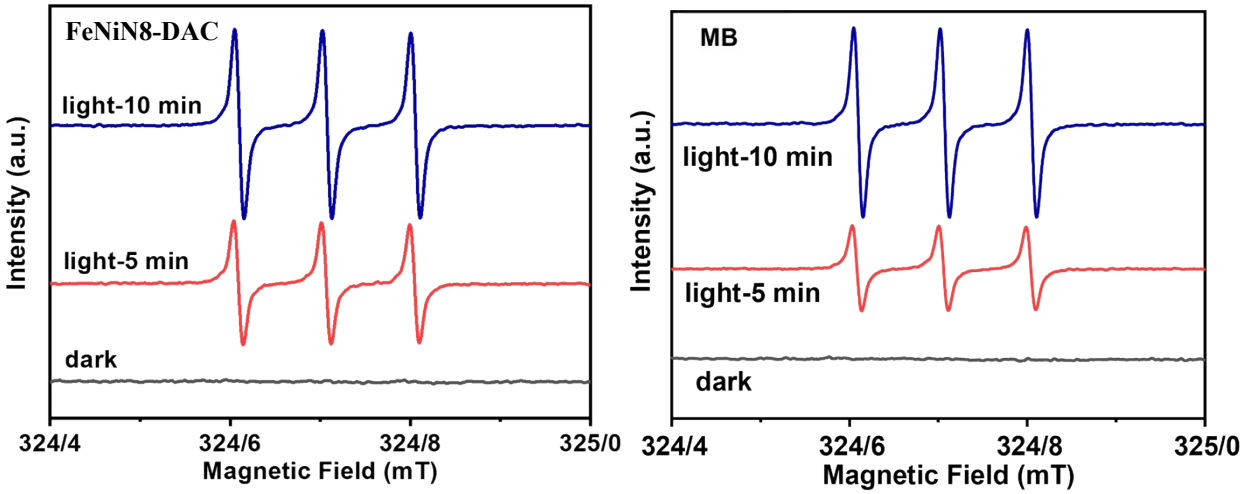

Figure S16. ESR spectra of N-doped, FeN4-SAC, CoN4-SAC, NiN4-SAC, FeNiN8-DAC, and methylene blue (MB, as the reference) without irradiation (dark) and with irradiations for 5 and 10 min in the presence of TEMP.

Singlet oxygen quantum yield of SACs ($\phi_{\Delta,SAC}$) was approximately calculated based on the results from ESR spectroscopy:

$$\phi_{\Delta,SAC} \approx \phi_{\Delta,MB} * \frac{I_{SAC}}{I_{MB}} \quad \text{(S1)}$$

in which I_{SAC} and I_{MB} are the peak intensity of ESR spectroscopy for SAC and methylene blue (MB, as the reference), respectively. $\phi_{\Delta,MB}$ is the quantum yield of MB in water (0.60).[2] The results are shown in **Figure S17**.

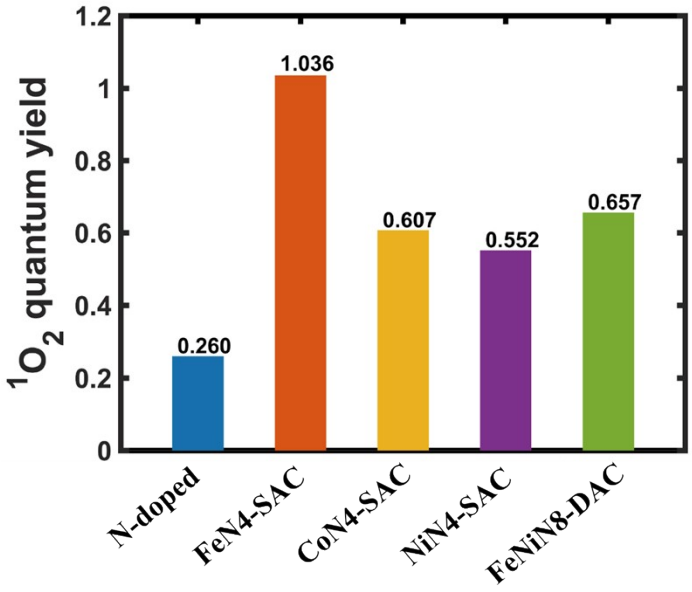

Figure S17. $^1O_2$ quantum yield of N-doped, FeN4-SAC, CoN4-SAC, NiN4-SAC, and FeNiN8-DAC samples obtained based on ESR results.

S3. Bandgap structure through Tauc plot and LEIPS analysis

Figure S18 shows the UV-Vis absorbance spectra of N-doped, FeN4-SAC, CoN4-SAC, NiN4-SAC, and FeNiN8-DAC samples. It is worth mentioning that the prepared SACs were totally dispersed into isopropanol during long sonication before doing UV-Vis characterizations to prevent light scattering.

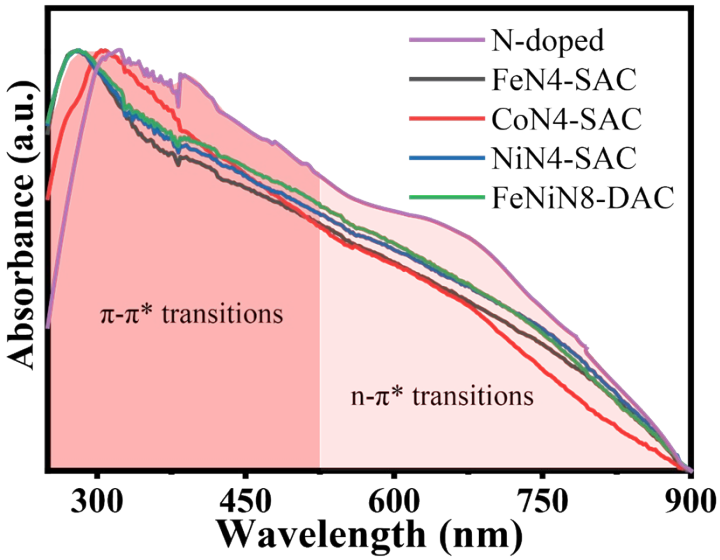

Figure S18. UV-Vis absorbance spectra of N-doped, FeN4-SAC, CoN4-SAC, NiN4-SAC, and FeNiN8-DAC samples.

In order to find the bandgap of SACs, we used Tauc relation:

$$(ahv)^{1/r} = \beta(hv - E_g) \qquad \text{(S2)}$$

Which r is 1/2 for direct allowed transitions. *a* is absorbance coefficient (a=2.303A/t) which A is the absorbance of the sample and t is the thickness of the sample. *hv* is the photon energy in eV (hv=1239/λ) and λ is the photon wavelength in nm. We can obtain the Tauc plot from UV-Vis spectra analysis for each sample as follows:

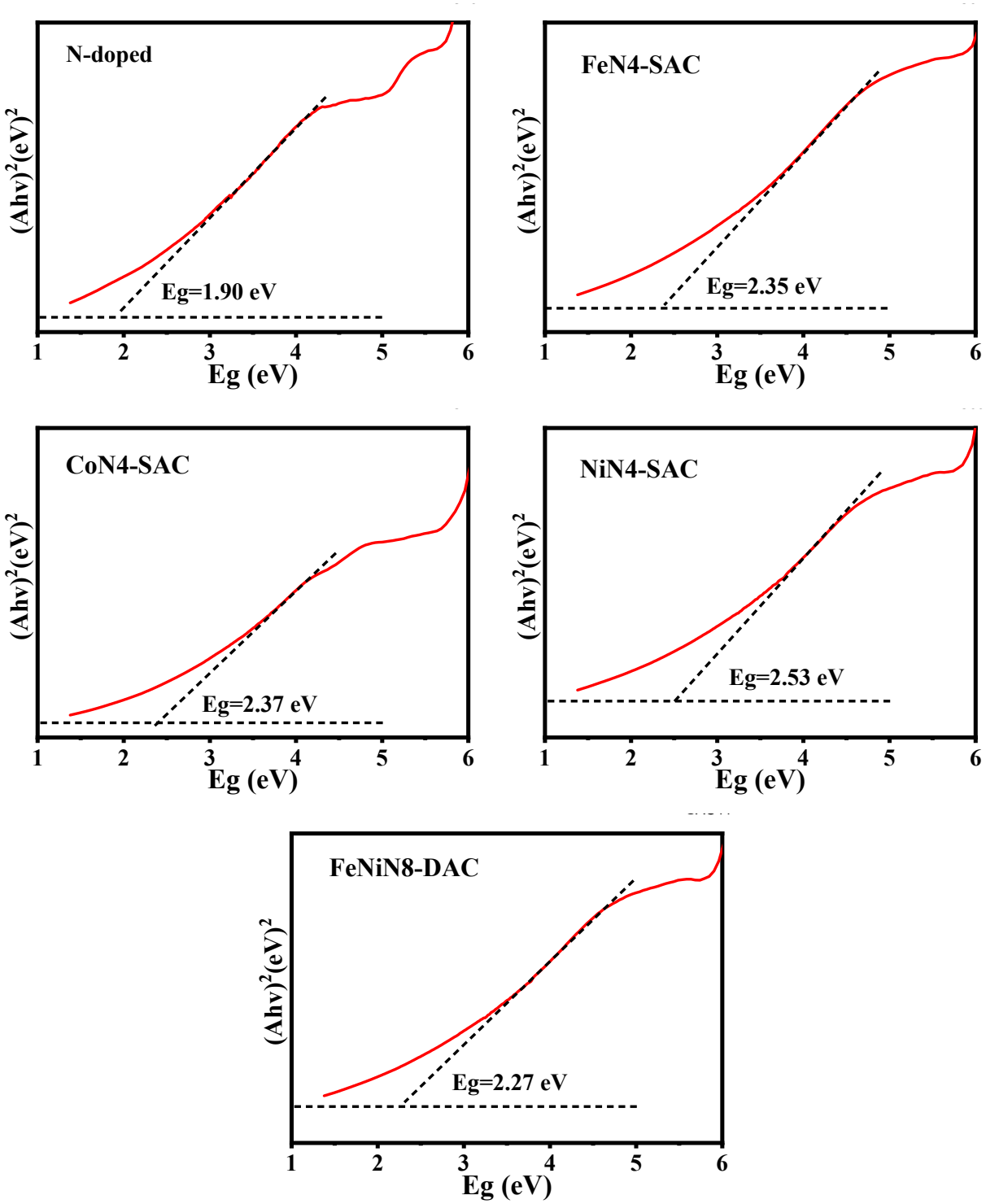

Figure S19. Optical Bandgap (E_g): Tauc plots of N-doped, FeN4-SAC, CoN4-SAC, NiN4-SAC, and FeNiN8-DAC samples. π-π* transitions were taken as primary to determine the materials' optical band gap (Eg).

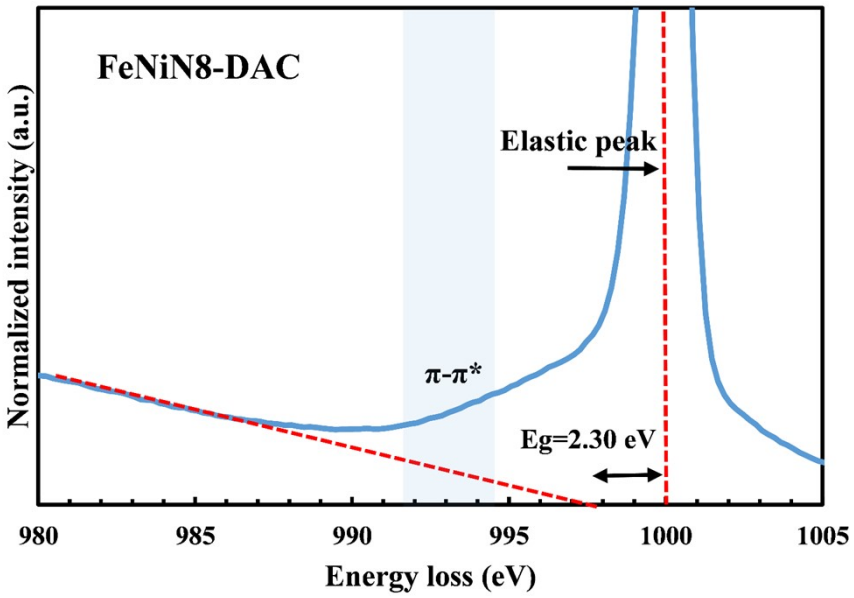

Figure S20. Reflection Electron Energy Loss Spectroscopy (REELS) of FeNiN8-DAC sample, leading to the bandgap (Eg) of 2.30 eV which agrees with optical bandgaps obtained from Tauc plots.

Low-Energy Inverse Photoemission Spectroscopy (LEIPS)[3] was performed to measure the valence band relative to the vacuum level for N-doped, FeN4-SAC, CoN4-SAC, NiN4-SAC, and FeNiN8-DAC samples. LEIPS analysis conditions are provided in **Table S1**.

Table S1. LEIPS (IPES) analysis conditions.

Sample bias	-9.0 V ~ -2.0 V (Electron Cathode: 9.6 V)
E-gun setting	3 uA (emission current) 40 V (extractor voltage)
Band Pass Filter	260/16-T55 (4.77 eV)
Energy step	0.04 eV
Time per step	2000 ms
Measurement time	~ 2 hr (10 scans)
Measured surface	As received

- PHI *in-situ* XPS/UPS/LEIPS measurement

LEIPS analysis for N-doped, FeN4-SAC, CoN4-SAC, NiN4-SAC, and FeNiN8-DAC samples are provided as follows:

1

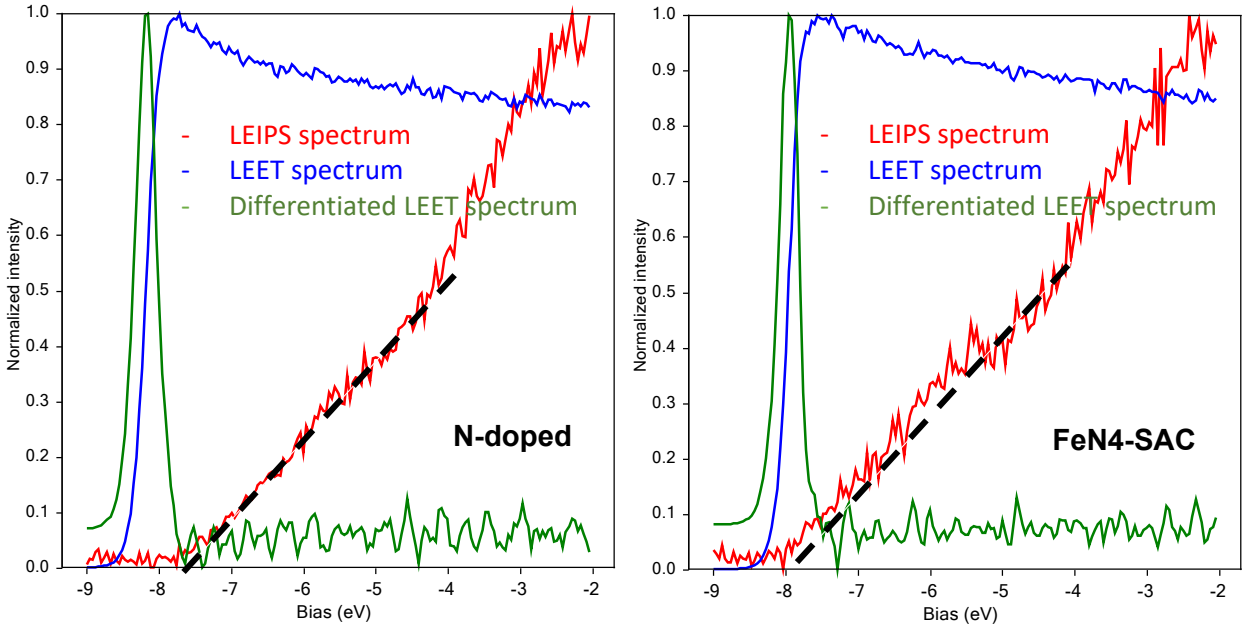
LEIPS spectrum
LEET spectrum
Differentiated LEET spectrum
N-doped
FeN4-SAC
Normalized intensity
Bias (eV)

2

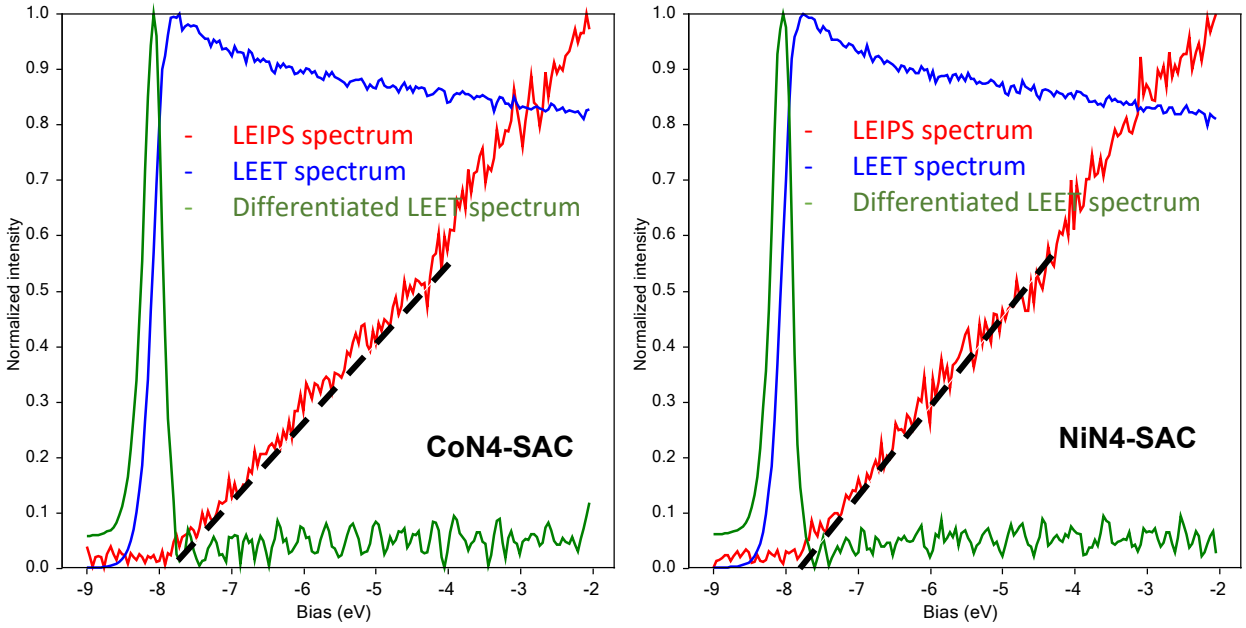
LEIPS spectrum
LEET spectrum
Differentiated LEET spectrum
CoN4-SAC
NiN4-SAC
Normalized intensity
Bias (eV)

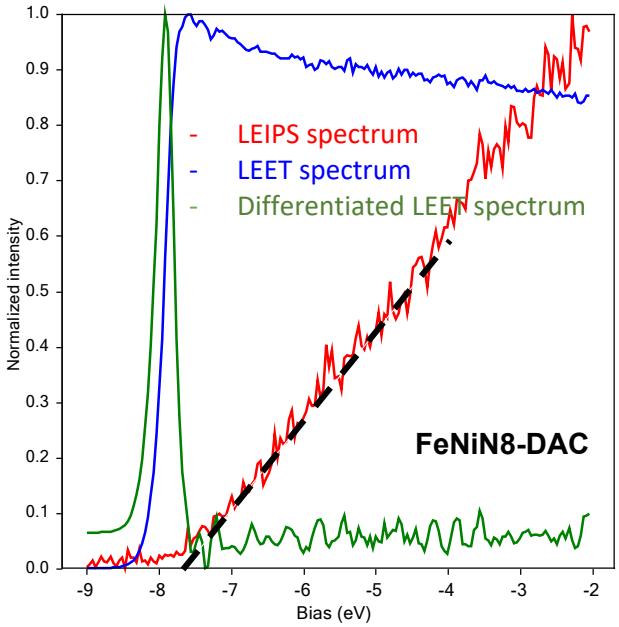

Figure S21. LEIPS analysis for N-doped, FeN4-SAC, CoN4-SAC, NiN4-SAC, and FeNiN8-DAC samples.

The radiative band-to-band recombination rate (R) is proportional to the np product:[4]

$$R = A\left(np - n_i^2\right) \tag{S3}$$

Where A is constant and:[5]

$$np = \gamma_n \gamma_p n_i^2 \exp\left(\frac{\Delta E_g}{k_B T}\right) \; and \; n_i^2 = N_c N_v \exp\left(-\frac{E_{g0}}{k_B T}\right) \tag{S4}$$

Where $\Delta E_g = E_{g0} + E_v - E_c$ and E_{g0} is the material band gap. In the nondegenerate limit, the Fermi-Dirac distribution reverts to the Maxwell-Boltzmann distribution and γ_n and γ_p are 1. So:

$$R = A n_i^2 \left(\exp\left(\frac{\Delta E_g}{k_B T}\right) - 1\right) \tag{S5}$$

And:

$$R = A N_c N_v \left(\exp\left(\frac{\Delta E_g}{k_B T}\right) - 1\right) \exp\left(-\frac{E_{g0}}{k_B T}\right) \tag{S6}$$

By increasing the material band gap (E_{g0}), the recombination rate (R) decreases.

1

S4. Triplet sensitization from TD-DFT calculations

Table S2. Electronic excitation energies (eV), oscillator strengths (*f*), and main configurations of the low-lying electronically excited states of SACs. Based on the optimized ground state geometry, the calculations are at the level of B3LYP and 6-31g(d,p) basis set [6] using Gaussian 09.

Sample	Excite state	Electronic transition	Excitation Energy (eV)	Oscillator strength (*f*)	Electronic component
N-doped	Singlet	$S_0 \rightarrow S_1$	1.086	0.0560	HOMO→LUMO (0.703)[a]
L-H=1.332 eV[b]	Singlet	$S_0 \rightarrow S_2$	1.391	0.0772	HOMO→LUMO+1 (0.664)
ΔE_{ISC}=0.367 eV[c]	Singlet	$S_0 \rightarrow S_3$	2.390	0.0000	HOMO→LUMO+2 (0.567)
	Triplet	$S_0 \rightarrow T_2$	0.719	0.0000	HOMO→LUMO+1 (0.700)
	Triplet	$S_0 \rightarrow T_1$	0.330	0.0000	HOMO→LUMO (0.737)
FeN4-SAC	Singlet	$S_0 \rightarrow S_4$[d]	1.445	0.0048	HOMO→LUMO (0.704)
L-H=2.372 eV	Singlet	$S_0 \rightarrow S_8$	2.524	0.0309	HOMO-1→LUMO+1 (0.672)
ΔE_{ISC}=0.040 eV	Singlet	$S_0 \rightarrow S_{10}$	2.582	0.0002	HOMO-1→LUMO+2 (0.641)
	Triplet	$S_0 \rightarrow T_2$	1.405	0.0000	HOMO-2→LUMO (0.682)
	Triplet	$S_0 \rightarrow T_1$	1.213	0.0000	HOMO→LUMO (0.698)
CoN4-SAC	Singlet	$S_0 \rightarrow S_2$	1.096	0.0059	HOMO→LUMO (0.701)
L-H=2.920 eV	Singlet	$S_0 \rightarrow S_4$	1.255	0.00034	HOMO→LUMO+1 (0.698)
ΔE_{ISC}=0.098 eV	Singlet	$S_0 \rightarrow S_6$	1.466	0.0009	HOMO→LUMO+2 (0.709)
	Triplet	$S_0 \rightarrow T_2$	0.998	0.0000	HOMO→LUMO (0.705)
	Triplet	$S_0 \rightarrow T_1$	0.931	0.0000	LUMO→LUMO+9 (0.621)
NiN4-SAC	Singlet	$S_0 \rightarrow S_4$	2.496	0.0369	HOMO→LUMO+2 (0.500)
L-H=2.890 eV	Singlet	$S_0 \rightarrow S_8$	2.672	0.00545	HOMO→LUMO+1 (0.691)
ΔE_{ISC}=0.126 eV	Singlet	$S_0 \rightarrow S_9$	2.786	0.2245	HOMO→LUMO+2 (0.482)
	Triplet	$S_0 \rightarrow T_2$	2.370	0.0000	HOMO-9→LUMO+3 (0.703)
	Triplet	$S_0 \rightarrow T_1$	2.276	0.0000	HOMO-1→LUMO+2 (0.637)
FeNiN8-DAC	Singlet	$S_0 \rightarrow S_6$	1.185	0.0041	HOMO→LUMO+1 (0.581)
L-H=1.346 eV	Singlet	$S_0 \rightarrow S_7$	1.315	0.0608	HOMO-1→LUMO+2 (0.528)
ΔE_{ISC}=0.108 eV	Singlet	$S_0 \rightarrow S_8$	1.367	0.0232	HOMO-2→LUMO+1 (0.494)
	Triplet	$S_0 \rightarrow T_2$	1.077	0.0000	HOMO-6→LUMO+1 (0.661)
	Triplet	$S_0 \rightarrow T_1$	1.067	0.0000	LUMO-1→LUMO+2 (0.525)
FeNiN6-DAC	Singlet	$S_0 \rightarrow S_8$	1.458	0.0288	HOMO-3→LUMO (0.513)
L-H=1.682 eV	Singlet	$S_0 \rightarrow S_9$	1.564	0.0328	HOMO-1→LUMO+1 (0.622)
ΔE_{ISC}=0.048 eV	Singlet	$S_0 \rightarrow S_{10}$	1.954	0.0436	HOMO-5→LUMO (0.393)
	Triplet	$S_0 \rightarrow T_2$	1.410	0.0000	HOMO-1→LUMO+1 (0.462)

	Triplet	$S_0 \rightarrow T_1$	1.298	0.000	LUMO-1→LUMO+1 (0.492)
Methylene blue	Singlet	$S_0 \rightarrow S_1$	2.591	0.9228	HOMO→LUMO (0.708)
L-H=2.488 eV	Singlet	$S_0 \rightarrow S_2$	2.758	0.0051	HOMO-1→LUMO (0.692)
ΔE_{ISC}=0.282 eV	Singlet	$S_0 \rightarrow S_3$	2.967	0.0016	HOMO-2→LUMO (0.706)
	Triplet	$S_0 \rightarrow T_2$	2.309	0.0000	HOMO-2→LUMO (0.695)
	Triplet	$S_0 \rightarrow T_1$	2.023	0.0000	HOMO-1→LUMO (0.700)

[a] The numbers in parentheses are the absolute value of coefficient of the wave function for each excitation.

[b] L and H stand for LUMO and HOMO, respectivly. L-H stands for the difference between LUMO and HOMO energies (eV).

[c] ΔE_{ISC} stands for the intersystem crossing gap energy.

[d] Please note that the singlet excited states with the oscillator strength of zero (such as S_1 to S_3) are not considered in the excitation process.[7]

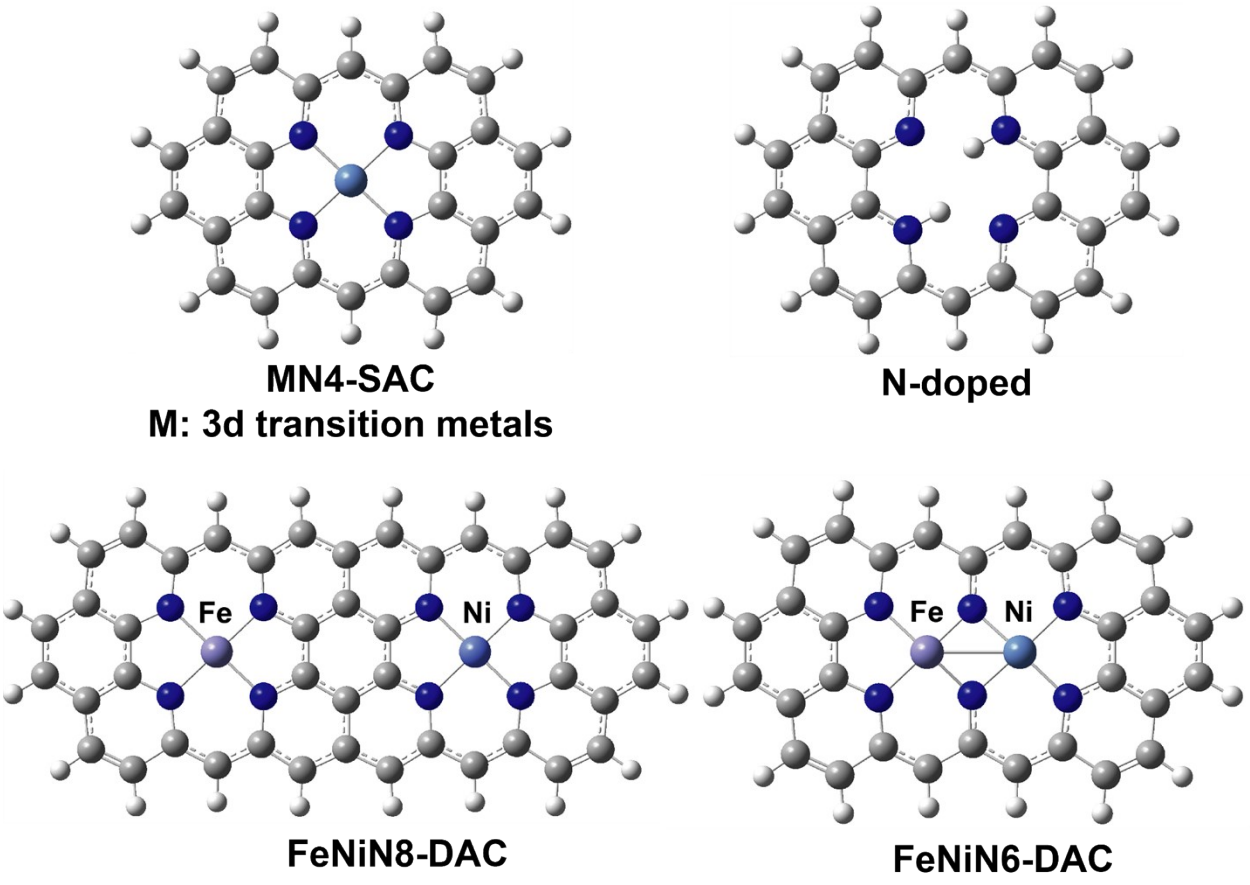

Figure S22. Optimized ground state structure of N-doped, MN4-SAC, FeNiN8-DAC, and FeNiN6-DAC samples from DFT calculation at the level of B3LYP and 6-31g(d,p) basis set using Gaussian 09.

Frontier molecular orbitals involved in excitation and singlet and triplet excited states of N-doped, FeN4-SAC, CoN4-SAC, NiN4-SAC, FeNiN8-DAC, and FeNiN6-DAC samples are provided in **Figure S23**.

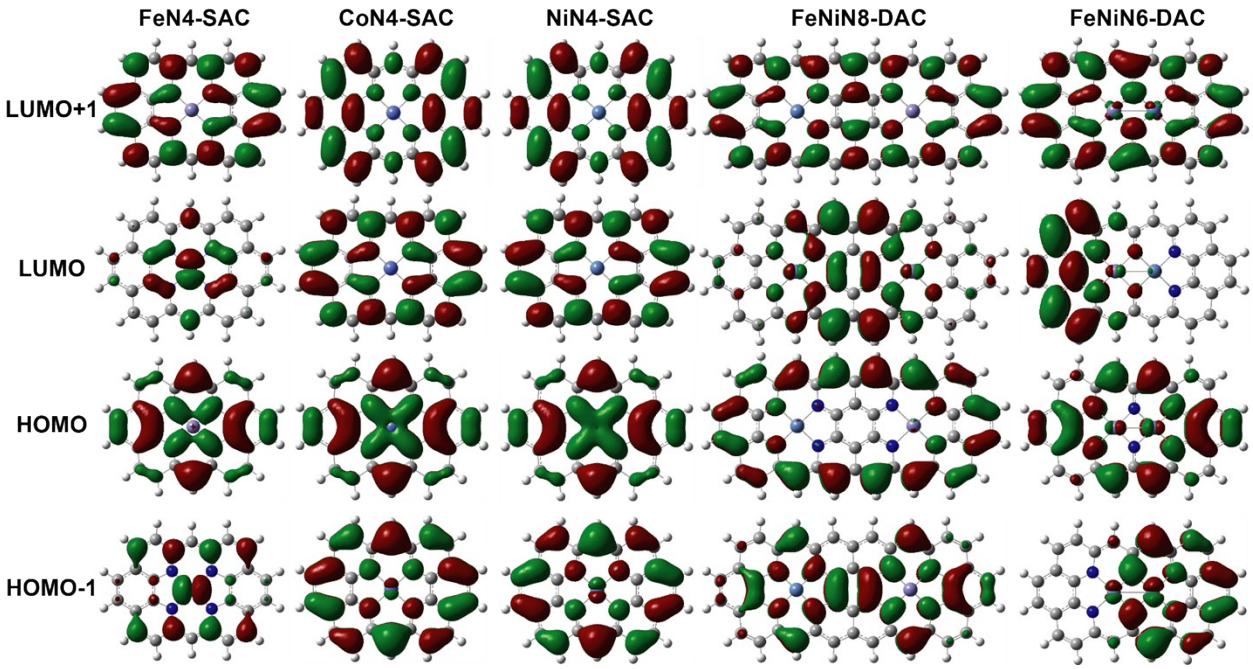

Figure S23. Frontier molecular orbitals involved in excitation and singlet and triplet excited states of N-doped, FeN4-SAC, CoN4-SAC, NiN4-SAC, FeNiN8-DAC, and FeNiN6-DAC samples (from DFT calculation at the level of B3LYP and 6-31g(d,p) basis set using Gaussian 09). Red and green colors represent electron availability and deficiency, respectively, with the isosurface value of 0.02 e/Å^3.

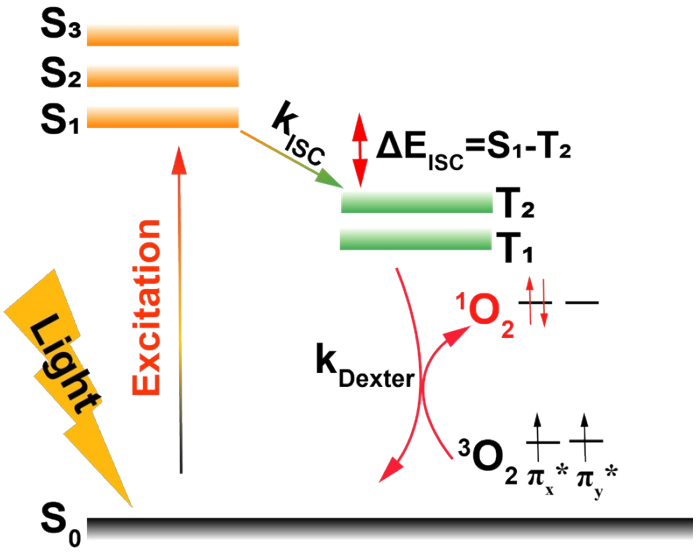

Figure S24. The schematic of Jablonski diagram for samples provided in Table S2, showing the singlet and triplet excited states based on optimized ground state (S_0) The calculations are at the level of TD-DFT/B3LYP/6-31g(d,p) using Gaussian 09.

S5. Multi-electron transfer process (Dexter energy transfer, DET) from DFT calculations

The rate of electron transfer (k_{Dexter}) can be described by the following equation:[8]

$$k_{Dexter} = KJexp\left(-\frac{2R}{L}\right) \quad \text{(S7)}$$

where K is a constant related to the specific donor-acceptor (SAC-O_2) couple, and J is the normalized spectral overlap between donor emission and acceptor absorption, which is independent of the oscillator strengths of the optical transitions. L is van der Waals radii, and R is the distance between donor and acceptor.[8] Because of the requirement for orbital overlap, Dexter transfer which is exponentially related to R, occurs typically on very short length scales (<10 Å). To calculate the distances between SAC and O_2 and to gain in-depth insight into the mechanism of $^1O_2$ generation through triplet-triplet energy transfer, DFT calculation was performed. **Figure S25** shows the schematic of Dexter electron transfer for triplet-triplet energy transfer:[9,10]

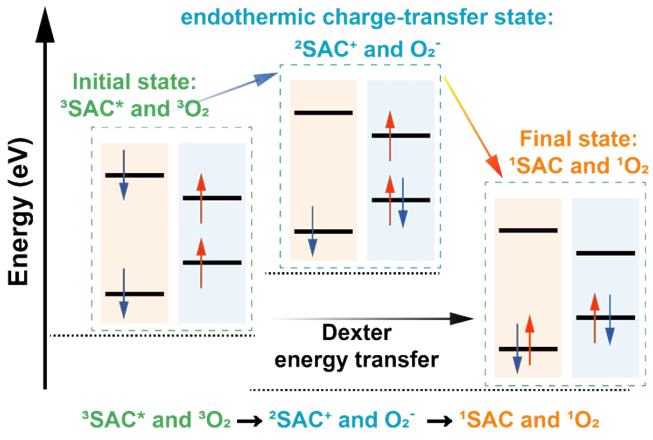

Figure S25. Schematic of Dexter electron transfer for triplet-triplet energy transfer.

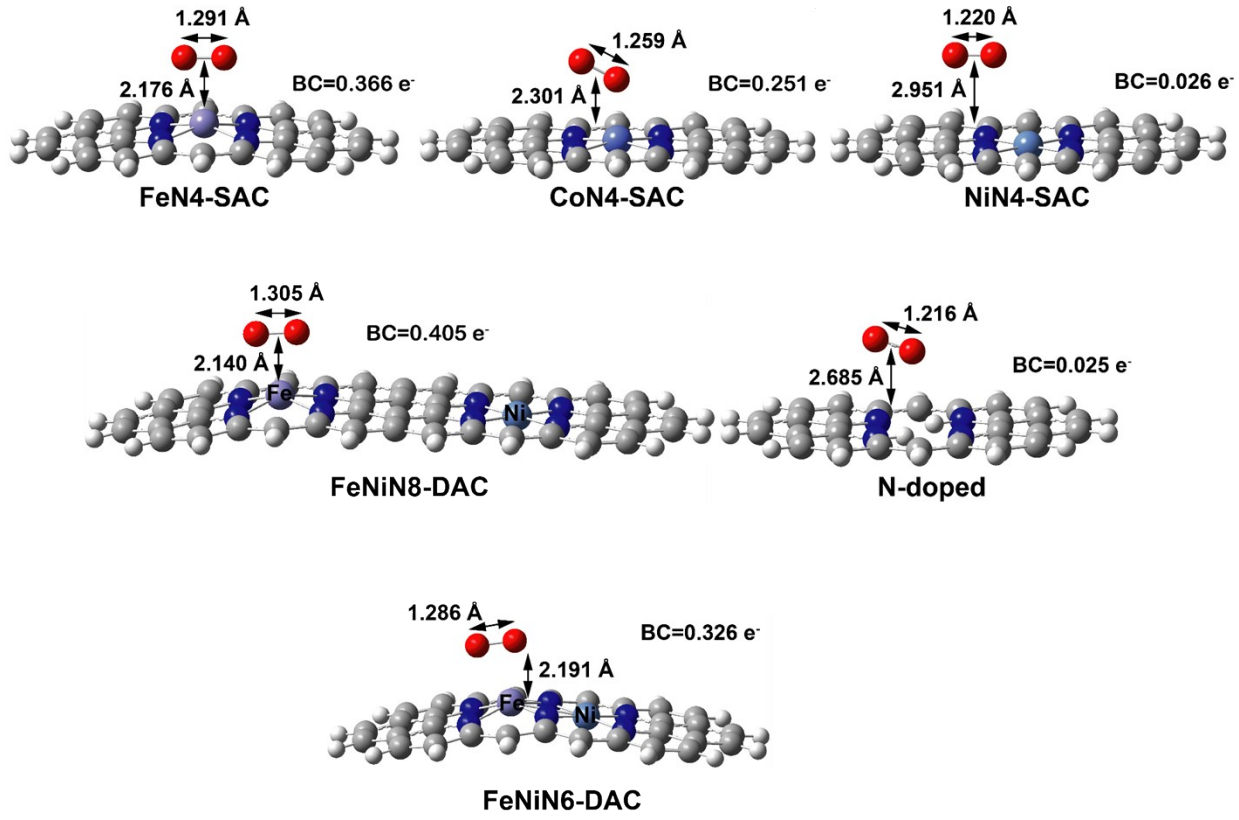

Figure S26. Adsorption of O_2 on N-doped, FeN4-SAC, CoN4-SAC, NiN4-SAC, FeNiN8-DAC, and FeNiN6-DAC, indicating the O−O bond length, the distance between SAC and O_2, and the charge transfer. BC stands for Bader charge.

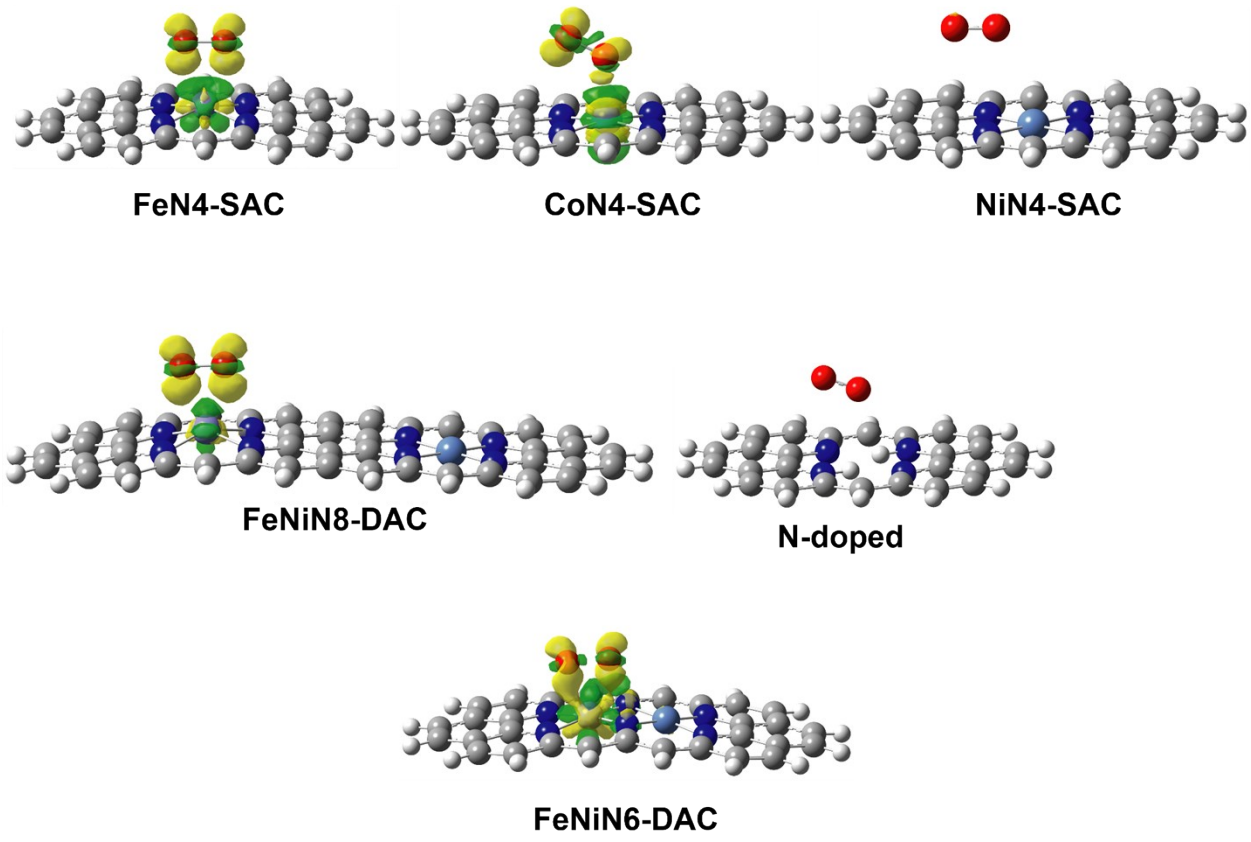

Figure S27. Charge transfer from N-doped, FeN4-SAC, CoN4-SAC, NiN4-SAC, FeNiN8-DAC, and FeNiN6-DAC to O_2 during adsorption. The yellow color represents electron availability while the green color represents electron deficiency, isosurface value = 0.0048 e/Å^3.

To further elucidate the electronic interactions between metals and absorbed O_2, the projected density of states (PDOS) for metals (Fe, Co, and Ni) 3d orbitals and O 2p orbitals are calculated. As shown **Figure S28**, more hybridization between 3d of Fe metal orbitals and 2p orbitals of dioxygen can be observed in contrast with Co and Ni metals. In addition, the contribution of the 3d orbital of metal atoms in the HOMO level is observed.

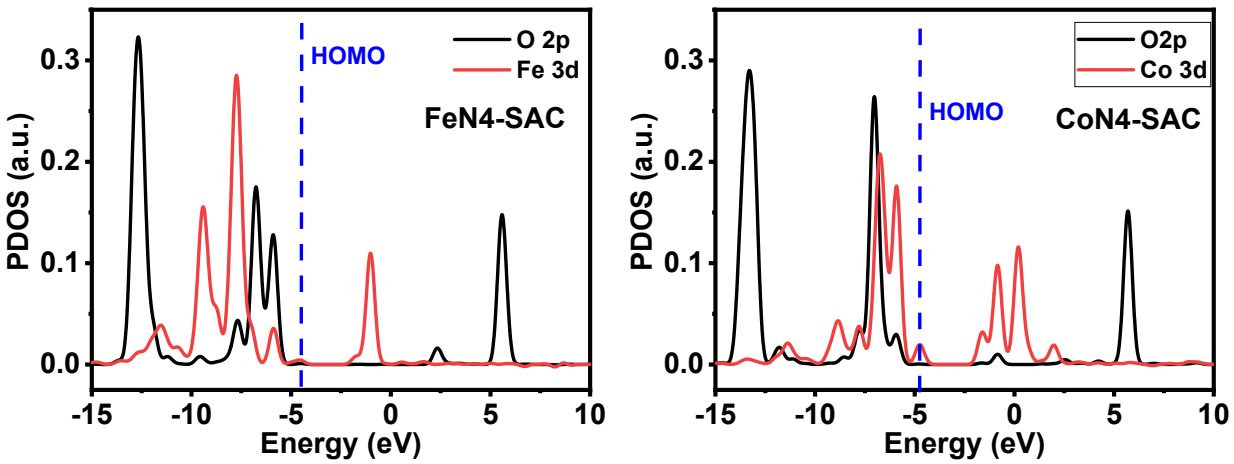

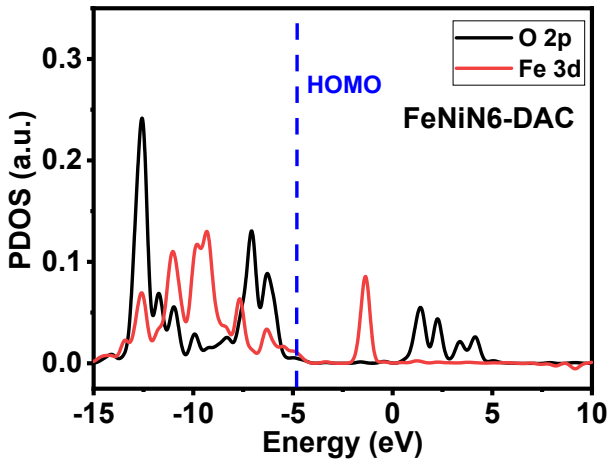

Figure S28. PDOS for the metal 3d (black line) and O 2p (red line) orbitals of N-doped, FeN4-SAC, CoN4-SAC, NiN4-SAC, FeNiN8-DAC, and FeNiN6-DAC samples. The population analysis is done using the Multiwfn program.[11]

Table S3. $^1O_2$ quantum yield, triplet sensitization, and electron transfer comparison of synthesized SACs obtained from ESR, TD-DFT, and DFT calculations, respectively.

sample	$^1O_2$ quantum yield[a]	ΔE_{ISC} (eV)[b]	O−O bond length (Å)	SAC−O distance (Å)	Charge transfer[c]
N-doped	0.260	0.367	1.217	2.685	0.025
FeN4-SAC	1.036	0.039	1.291	2.176	0.366
CoN4-SAC	0.607	0.098	1.259	2.301	0.251
NiN4-SAC	0.552	0.126	1.220	2.951	0.022
FeNiN8-DAC	0.657	0.108	1.305	2.140	0.405
FeNiN6-DAC	--[f]	0.048	1.286	2.191	0.326

[a] $^1O_2$ quantum yield is obtained from ESR
[b] ΔE_{ISC} (eV) is calculated from TD-DFT calculations
[c] charge transfer is calculated from DFT calculations
[f] experiments are not done for FeNiN6-DAC

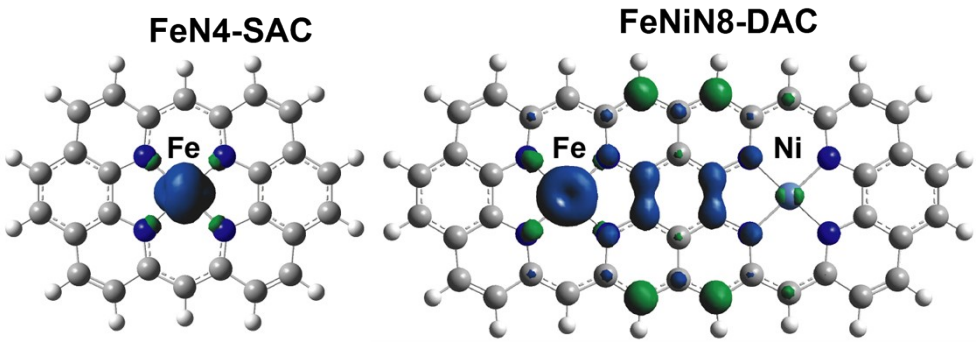

Figure S29. Spin density of FeN4-SAC and FeNiN8-DAC samples, indicating the delocalization of unpaired electrons of high-lying d_{z2} orbital of Fe atom into ligands. The blue color represents alpha spin while the green color represents beta spin, isosurface value = 0.004 e/Å^3.

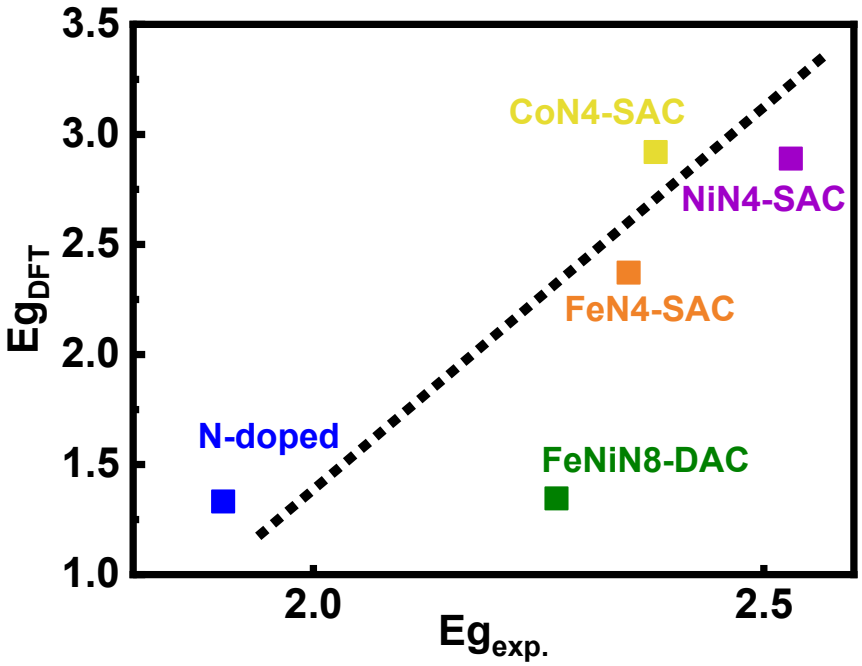

Figure S30. DFT-predicted bandgap (Eg) versus experimental Eg.

S6. Rate of $^1O_2$ sensitization

Based on equation S7, the rate of triplet-triplet energy transfer through Dexter energy transfer is defined. On the other hand, the Arrhenius equation provides the rate constant for triplet sensitization (k_{ISC}):

$$k_{ISC} = Aexp\left(-\frac{\Delta E_{ISC}}{kT}\right) \quad \text{(S8)}$$

where A is the pre-exponential factor, k is the Boltzman constant, T is the absolute temperature (in degrees Kelvin), and ΔE_{ISC} is the intersystem crossing energy gap (activation energy, eV). So the rate of $^1O_2$ sensitization can be defined as follows:

$$K_{1_{O_2}} = k_{Dexter}^{\alpha} k_{ISC}^{\beta} = A^{\alpha} exp\left(-\alpha\frac{\Delta E_{ISC}}{kT}\right)(KJ)^{\beta} exp\left(-\beta\frac{2R}{L}\right) \quad \text{(S9)}$$

and

$$K_{1_{O_2}} \propto exp\left(-\alpha\frac{\Delta E_{ISC}}{kT} - \beta\frac{2R}{L}\right) \quad \text{(S10)}$$

This universal equation shows the synergy effect of triplet sensitization and electron transfer applicable for SACs and DSACs. This equation indicates that by decreasing both R and ΔE_{ISC}, the rate of $^1O_2$ sensitization increases. Hence at R=2.176 Å and ΔE_{ISC}=0.039 eV, $K_{1_{O_2}}$ is enhanced for FeN4-SAC.

S7. Machine Learning (ML) for prediction of Gibbs free energy (ΔG)

Input data collection

The data used for the training of ML model is collected from the literature. The data contains the 2084 data points for the Gibbs free energy (ΔG) of reaction intermediates such as OH*, O*, OOH*, O_2*, H*, CO_2*, COOH*, CO*, and N_2*. The data is based on the 3d, 4d, and 5d transition metals on graphene and porphyrin supports. The data are sorted in an excel file in such a way that the input features, the SACs structure, and the Gibbs free energies are provided for the training of ML algorithm (please see the Supporting Information). **Figure S31** shows the violin plot of Gibbs free energy (ΔG, eV) distribution for H*, N_2*, OH*, O*, OOH*, CO*, and COOH* reaction intermediates. The violin plot displays also the number of datapoints for each reaction intermediates leading to a total of 2084 input data. The Gibbs free energy is distributed from -4 eV to 7 eV. More specifically, the Gibbs free energy of OOH* intermediate is between 0 to 7 eV with the average of around 4 eV and the mode of around 5.5 eV.

Machine Learning training

We apply support vetor regression (SVR) model to construct the structure-activity relationship and perform further analysis on the predicted data. **Figure S32a** shows the flowchart for the construction of SVR model based on the hyperparameters tuning using Bayesian optimization along with 10-fold cross validation (CV). First, the input data was randomly partitioned into the train set (90%, 1876 data points) and test set (10%, 208 data points). The input features were normalized by the MinMaxScaler function of Sklearn, and the initial guess for the hyperparameters of SVR algorithm (C and gamma) were given to the model. The optimized value for the

hyperparameters were predicted using Bayesian optimization by minimizing the mean absolute error (MAE) of test set as the activation function. **Scheme S32b** shows the top view and lateral view of the structure of a typical SAC along with the list of input features including the properties of transition metal, substrate, and intermediates.

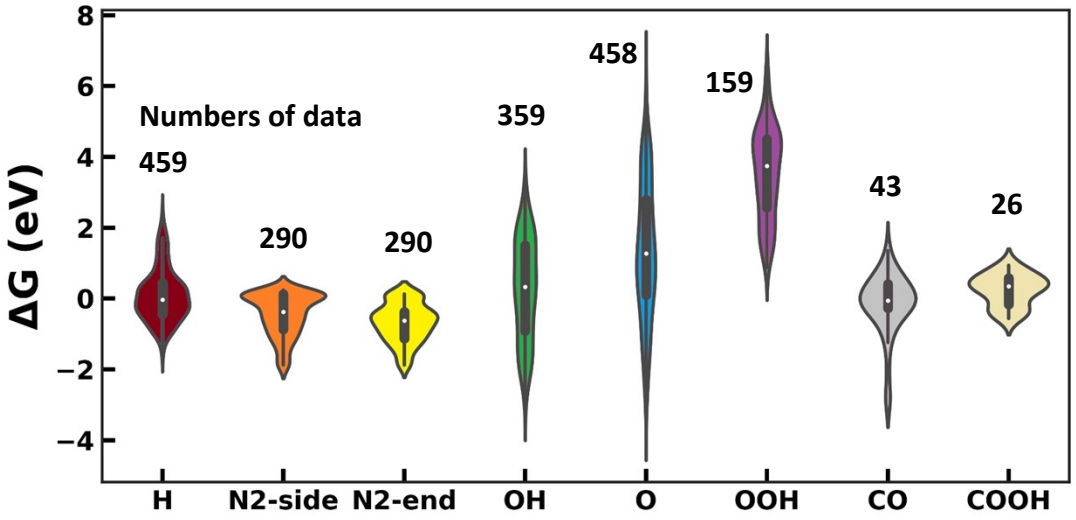

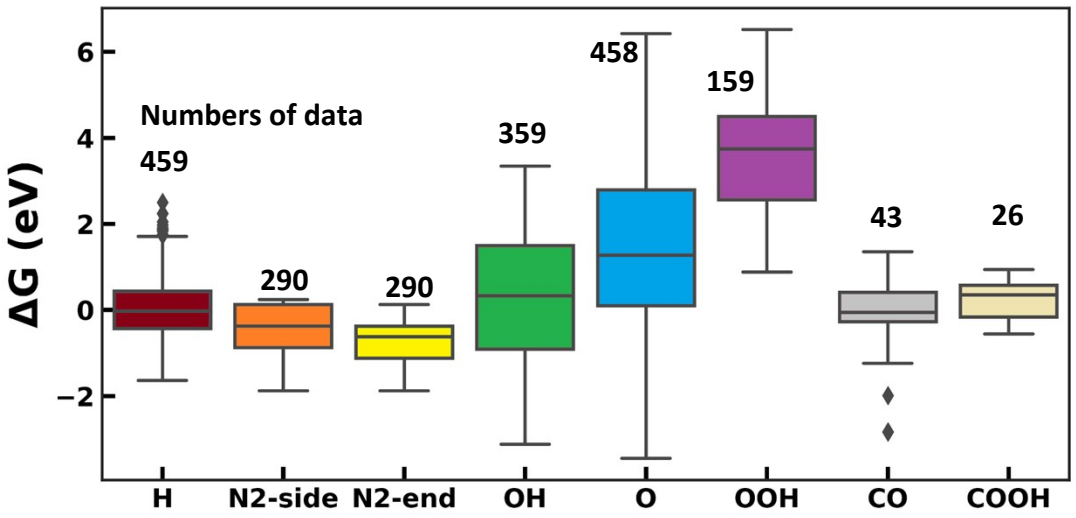

Figure S31. Distribution of training data for machine learning (ML). Violin plot (a) and box plot (b) of input data distribution for H*, N_2*, OH*, O*, OOH*, CO*, and COOH* intermediates.

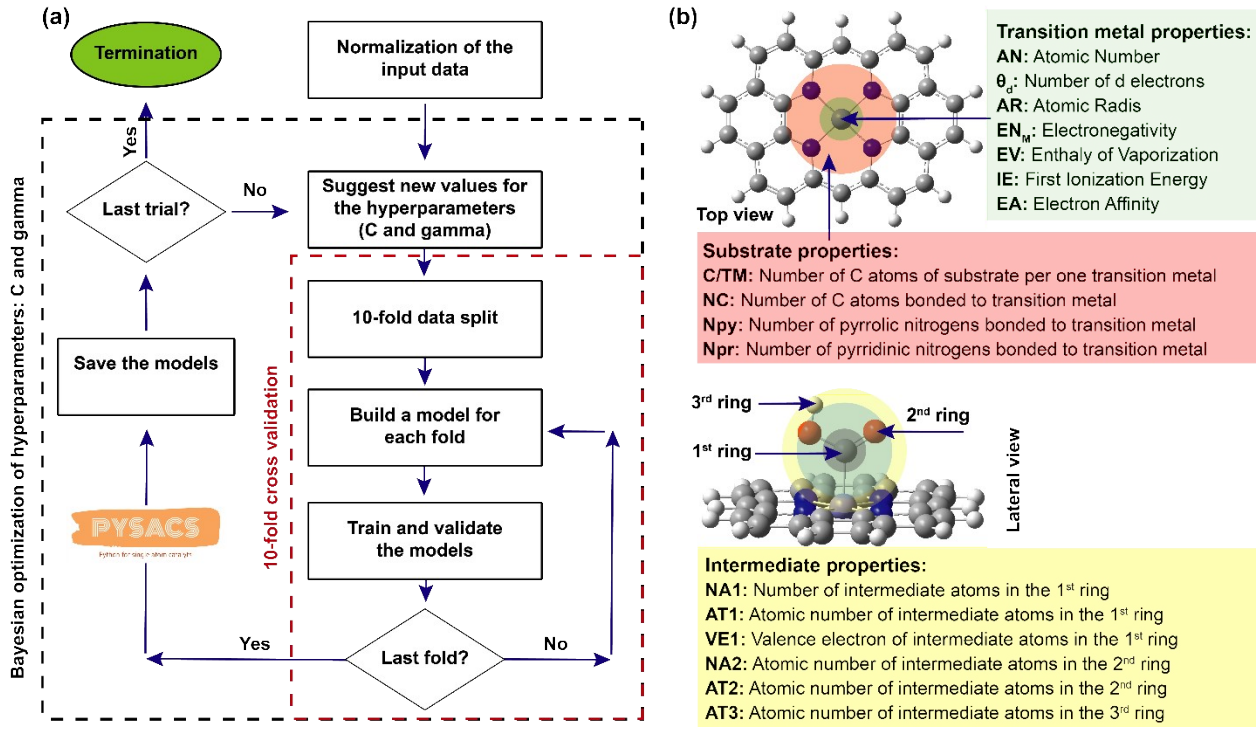

Figure S32. Construction of ML for the design of single atom catalyst. (a) Flowchart for the automated hyperparameters tuning of the support vector regression (SVR) model using Bayesian optimization and 10-fold cross validation (CV). (b) Top view and lateral view of the structure of single atom catalyst (SACs) along with the input features including the properties of transition metal, substrate, and intermediates.

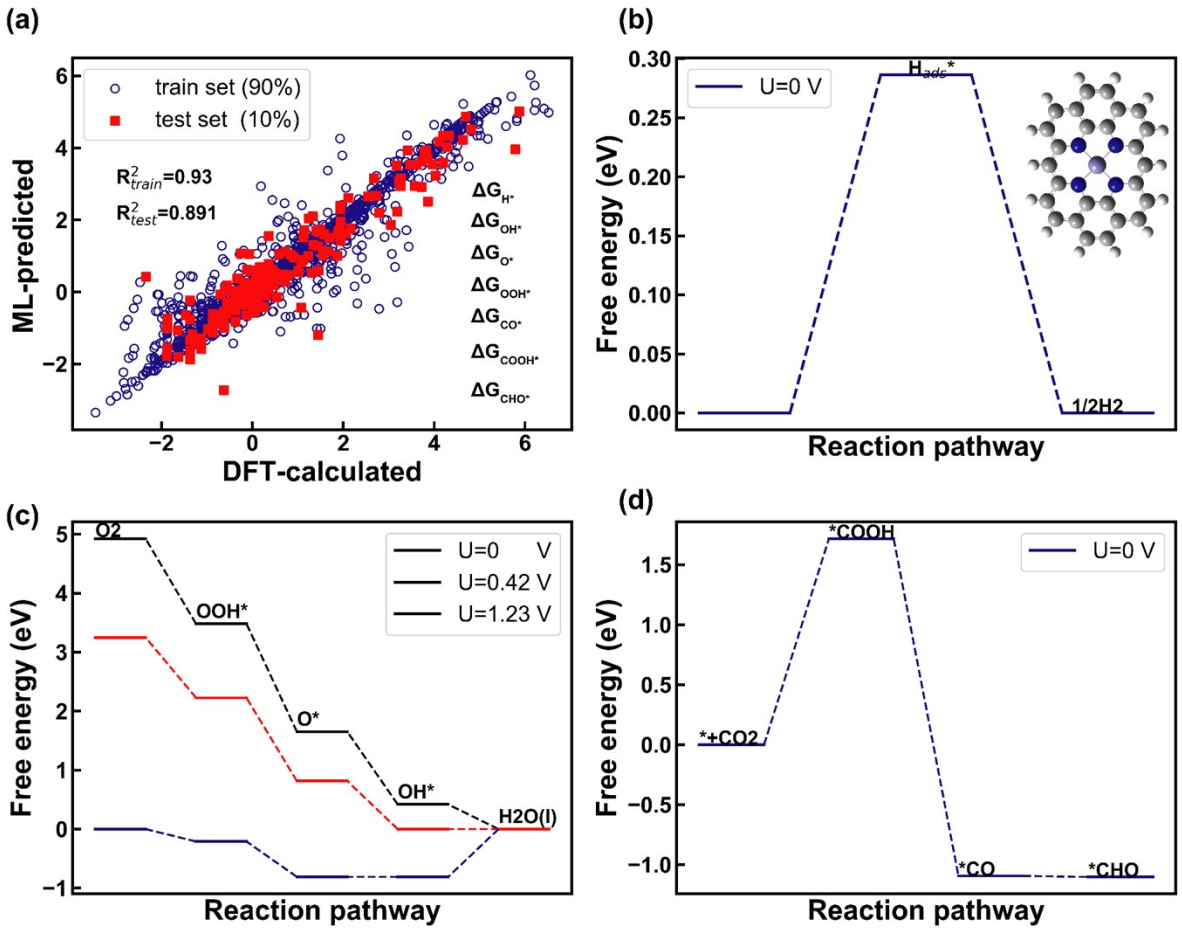

Figure S33. Performance prediction. (a) Calculated adsorption energies of reaction intermediates such as H*, OH*, O*, OOH*, CO*, COOH*, and CHO* using the advanced ML method versus the DFT method. (b-d) Free energy diagram predicted for HER, ORR, and CO_2RR for FeN4-SAC.

S8. References

(1) Eckmann, A.; Felten, A.; Verzhbitskiy, I.; Davey, R.; Casiraghi, C. Raman Study on Defective Graphene: Effect of the Excitation Energy, Type, and Amount of Defects. *Phys. Rev. B - Condens. Matter Mater. Phys.* **2013**, *88* (3), 1–11. https://doi.org/10.1103/PhysRevB.88.035426.

(2) Wilkinson, F.; Helman, W. P.; Ross, A. B. Quantum Yields for the Photosensitized Formation of the Lowest Electronically Excited Singlet State of Molecular Oxygen in Solution. *J. Phys. Chem. Ref. data* **1993**, *22* (1), 113–262.

(3) Yoshida, H. Near-Ultraviolet Inverse Photoemission Spectroscopy Using Ultra-Low Energy Electrons. *Chem. Phys. Lett.* **2012**, *539–540*, 180–185. https://doi.org/10.1016/j.cplett.2012.04.058.

(4) Band to Band Radiative Recombination https://www.sciencedirect.com/topics/engineering/band-to-band-radiative-recombination.

(5) Recombination and Generation https://doc.comsol.com/5.5/doc/com.comsol.help.semicond/semicond_ug_semiconductor.6.54.html.

(6) Paul, P.; Mati, S. S.; Bhattacharya, S. C.; Kumar, G. S. Exploring the Interaction of Phenothiazinium Dyes Methylene Blue, New Methylene Blue, Azure A and Azure B with TRNAPhe: Spectroscopic, Thermodynamic, Voltammetric and Molecular Modeling Approach. *Phys. Chem. Chem. Phys.* **2017**, *19* (9), 6636–6653. https://doi.org/10.1039/c6cp07888e.

(7) Wu, W.; Zhang, Q.; Wang, X.; Han, C.; Shao, X.; Wang, Y.; Liu, J.; Li, Z.; Lu, X.; Wu, M. Enhancing Selective Photooxidation through Co−Nx-Doped Carbon Materials as Singlet Oxygen Photosensitizers. *ACS Catal.* **2017**, *7* (10), 7267–7273. https://doi.org/10.1021/acscatal.7b01671.

(8) Tabachnyk, M.; Ehrler, B.; Gélinas, S.; Böhm, M. L.; Walker, B. J.; Musselman, K. P.; Greenham, N. C.; Friend, R. H.; Rao, A. Resonant Energy Transfer of Triplet Excitons from Pentacene to PbSe Nanocrystals. *Nat. Mater.* **2014**, *13* (11), 1033–1038.

https://doi.org/10.1038/NMAT4093.

(9) Luo, X.; Han, Y.; Chen, Z.; Li, Y.; Liang, G.; Liu, X.; Ding, T.; Nie, C.; Wang, M.; Castellano, F. N.; Wu, K. Mechanisms of Triplet Energy Transfer across the Inorganic Nanocrystal/Organic Molecule Interface. *Nat. Commun.* **2020**, *11* (1), 1–10. https://doi.org/10.1038/s41467-019-13951-3.

(10) Lai, R.; Liu, Y.; Luo, X.; Chen, L.; Han, Y.; Lv, M.; Liang, G.; Chen, J.; Zhang, C.; Di, D.; Scholes, G. D.; Castellano, F. N.; Wu, K. Shallow Distance-Dependent Triplet Energy Migration Mediated by Endothermic Charge-Transfer. *Nat. Commun.* **2021**, *12* (1), 1–9. https://doi.org/10.1038/s41467-021-21561-1.

(11) Lu, T.; Chen, F. Multiwfn: A Multifunctional Wavefunction Analyzer. *J. Comput. Chem.* **2012**, *33* (5), 580–592. https://doi.org/10.1002/jcc.22885.